Comparison of Solar Oscillation Frequencies obtained from the Multiple-Peak, Tesseral-Spectrum Method, and Established Fitting Methodologies in Helioseismology

Johann Reiter,[1] Edward J. Rhodes, Jr.,[2] Jesper Schou,[3] Timothy P. Larson,[4] and Philip H. Scherrer[4]

[1]*Zentrum Mathematik M17*

Technische Universität München

D-85748 Garching bei München, Germany

[2]*Department of Physics and Astronomy*

University of Southern California

Los Angeles, CA 90089-1342, USA

[3]*Max-Planck-Institut für Sonnensystemforschung*

D-37077 Göttingen, Germany

[4]*W. W. Hansen Experimental Physics Laboratory*

Stanford University

Stanford, CA 94305-4085, USA

ABSTRACT

Analysis of the frequencies of solar global oscillations allows the investigation of the internal structure of the Sun. An important test of the reliability of the mode frequencies obtained from various fitting methodologies is that they are consistent with one another when applied to contemporaneous helioseismic observations. Here we compare f- and p-mode frequencies obtained from the Multiple-Peak, Tesseral-Spectrum Method (MPTS, Reiter et al. 2020) with those obtained from the Mean-multiplet technique (JS, Schou 1992), the high-degree fitting methodology of Korzennik (SKh, Korzennik et al. 2004), the medium-degree methodology of Korzennik (SKm, Korzennik 2005, 2008a,b), and the fitting methodology of the Birmingham Solar Oscillations Network group (BR, Broomhall et al. 2009). The data analyzed in this study are based on 67-, 72-, and 90-day long time series of full-disk doppler-grams acquired by the HMI in 2010, and on low-degree Sun-as-a-star observations acquired by the ground-based observing stations of the BiSON group. While we find excellent agreement between the MPTS, JS, SKm, and BR frequencies, we also find significant differences between both the MPTS and JS frequencies and the SKh frequencies. We also demonstrate that the systematic differences between theMPTS(67d) and SKh(67d) high-degree frequencies are not due to the use of invalid seed frequencies in the MPTS method.

Keywords: The Sun (1693) — Helioseismology (709)

1. INTRODUCTION

Since the advent of helioseismology in the mid-1970s, extensive helioseismic data has been acquired both from earth-bound networks of observatories as well as from space-borne missions that has made it possible to gain important insights on solar structure, rotation, and their temporal variations (Christensen-Dalsgaard 2002; Kosovichev 2009; Basu 2010, 2016). In most cases observations of the Doppler-shifted line-of-sight velocity are carried out, extending over months or even years to achieve a high frequency resolution.

Observing the Sun as a star in disk-integrated light, low-degree modes have been studied in great detail with both the BiSON (Birmingham Solar Oscillations Network) (Chaplin et al. 1996; Hale et al. 2016) and the IRIS (International Research on the Interior of the Sun) (Fossat 1991) networks as well as with the GOLF (Global Oscillations at Low

Frequency) instrument (Gabriel et al. 1997) onboard the SOHO (Solar and Heliospheric Observatory) spacecraft. Since late 1995 the six-station Global Oscillation Network Group (GONG) network (Harvey et al. 1996, 1998; Hill et al. 2003) has provided nearly continuous data for modes of degrees up to about 150. Modes including even higher degrees were extensively studied within the framework of the Solar Oscillations Investigation (SOI) with the Michelson Doppler Imager (MDI) instrument (Scherrer et al. 1995) onboard the SOHO spacecraft , but these high-resolution data were only available a few months each year. Since May 2010, MDI has been superseded by the Helioseismic and Magnetic Imager (HMI) (Schou et al. 2012) of the Solar Dynamics Observatory (SDO) space-borne mission, while the regular MDI observations were discontinued in April 2011.

Broomhall et al. (2009) and Davies et al. (2014) performed detailed analyses of the BiSON low-degree observations, while Larson & Schou (2015, 2018) analyzed the MDI and HMI observations for modes of degrees up to 300. High-degree MDI and HMI observations were analyzed, in particular, by Rhodes et al. (1997); Korzennik et al. (2004); Reiter et al. (2015) and Reiter et al. (2020).

In contrast to the estimation of low- and intermediate-degree mode parameters, the determination of high-degree mode parameters turns out to be difficult, because high-degree modes cannot be observed as sharp, isolated peaks but only as ridges of power comprised of overlapping modes. Aggravating the situation, the central frequency of each ridge deviates from the frequency of the target mode, because of the asymmetrical distribution of the amplitudes of the modes that blend together. Hence, to recover the underlying mode frequency from fitting the ridge, an accurate model of the ridge power as a function of frequency is indispensable, as has been pointed out by Korzennik et al. (2004) and Reiter et al. (2015). On the other hand, because high-degree modes have their lower turning-point radius quite close to the surface, they are extremely interesting for the study of the near-surface layers (see, for example, Di Mauro et al. 2002; Basu 2016), where thermodynamic effects associated with helium and hydrogen ionization become relevant.

Using data that were acquired during the 2010 Dynamics Run of the MDI, Reiter et al. (2020) have compared in a pre-liminary comparative study both their windowed, multiple peak, averaged-spectrum (WMLTP) method (Reiter et al. 2015) and multiple-peak, tesseral spectrum (MPTS) method (Reiter et al. 2020) with both the mean-multiplet technique of Schou (1992) and the high-degree fitting methodology of Korzennik et al. (2004) in terms of the fitted frequencies, line widths, and a_1 frequency-splitting coefficients. While there was an excellent agreement between the MPTS method and the mean-multiplet technique, systematic deviations resulted in particular in the convection zone between the MPTS method, the WMLTP method, and the high-degree fitting methodology of Korzennik et al. (2004) (see Figures 19 and 20 in Reiter et al. (2020)). In the present paper we will report the results of a detailed comparative study between the MPTS method (Reiter et al. 2020), the mean-multiplet technique (Schou 1992), the high-degree fitting methodology of Korzennik et al. (2004), the medium-degree fitting methodology of Korzennik (2005, 2008a,b), and the fitting methodology of the Birmingham Solar Oscillations Network group (Broomhall et al. 2009) in terms of frequencies. In particular, it will be shown that the MPTS method is able, at least for the lower-order ridges, to accurately restore the MPTS frequencies, MPTS(67d), obtained in 2010 from a 67-day long observing run of the HMI, when starting from the frequencies, SKh(67d), obtained from the high-degree fitting methodology of Korzennik et al. (2004).

For a comparison of p-mode parameters from MDI and GONG we refer to Schou et al. (2002) and Basu et al. (2003), and from BiSON and GONG to Howe et al. (2003).

The present paper is organized as follows. After a brief presentation in Section 2 of the fitting methodologies included in our comparative study, we describe in Section 3 the origin of the data used. In Section 4 we present the results from our comparitive study. In Section 5 we demonstrate that the differences in the SKh(67d) and MPTS(67d) frequencies are not due to the use of invalid seed frequencies in the MPTS method. Our concluding remarks are given in Section 6.

2. FITTING METHODOLOGIES

Before we will present the results from our comparative study, we comment briefly on the various methods involved. Where resolved data are available, timeseries of spherical harmonic coefficients are used, which result from the spatial decomposition of the individual Dopplergrams in an observing run.

2.1. MPTS method

The MPTS method of Reiter et al. (2020) is equally well-suited for the estimation of low-, medium-, and high-degree f- and p-mode parameters and frequency-splitting coefficients. In the MPTS method a theoretical multiple-peak profile, $M_{n,l,m}(\nu)$, based upon the asymmetrical profile of Nigam & Kosovichev (1998) is employed to represent the

distribution of power with frequency, ν, of an oscillation peak of n, l, and m. This theoretical profile is composed of the profile of the targeted peak (n, l, m), the sum of the profiles of the l- and m-leaks of radial order n, the sum of the leaks from multiplets other than (n, l), and a background that is quadratic in frequency. The amplitudes of the l- and m-leaks relative to the amplitude of the targeted mode (n, l, m) are assumed to be given by the leakage matrix which is corrected for the distortion that is caused by the solar differential rotation, according to the theory of Woodard (1989). Because the power in a single frequency bin of a power spectrum obeys an exponential rather than a Gaussian distribution, as in the case of an m-averaged spectrum for degrees $l \gg 1$, a maximum-likelihood approach is employed in the MPTS method for fitting the theoretical multiple-peak profile $M_{n,l,m}(\nu)$ to an observed power spectrum in a suitably chosen fitting box around the targeted peak (n, l, m). Since the MPTS method operates directly upon of all the $2l + 1$ modes in a multiplet (n, l), $2l + 1$ sets of modal parameters are obtained simultaneously for that multiplet (n, l). By simply averaging all of the $2l + 1$ frequency estimates within a multiplet, the average frequency for that multiplet is obtained, which is called the "mean-multiplet frequency". In addition, by fitting an appropriate polynomial to the run of the fitted frequencies versus m, the frequency-splitting coefficients for that multiplet are estimated, and are used for the correction of the leakage matrix for that multiplet by calculating the expansion coefficients B_2 and B_4 of the solar differential rotation.

In the following we will use the term "MPTS" when we are referring to the MPTS method.

2.2. *Mean-multiplet technique*

In the mean-multiplet technique of Schou (1992) (see also Schou et al. 2002) Fourier transforms of the spherical harmonic timeseries are fit using a maximum likelihood approach, taking into account leakage between the modes (Larson & Schou 2015). Rather than fitting, however, for the individual $2l + 1$ mode frequencies within a multiplet (n, l), this technique includes a fitting algorithm that yields the mean-multiplet frequency $\nu_{n,l}$ and the set of frequency-splitting coefficients $a_k^{(n,l)}$ for each multiplet directly, assuming that the line width of the $2l + 1$ modes within the multiplet is independent of the azimuthal order m, while the relative variation of the mode amplitudes with m is assumed to be given by the leakage matrix which is corrected, according to the theory of Woodard (1989), for the distortion that is caused by the solar differential rotation. This correction of the leakage matrix is done for each multiplet (n, l) by calculating the expansion coefficients B_2 and B_4 of the solar differential rotation from the frequency-splitting coefficients obtained for that multiplet. Initially, the algorithm fits for a total of 6 frequency-splitting coefficients, then for 18 and 36 once the 6-term fits have converged. Leaks from multiplets other than (n, l) are calculated from the mode parameters for those modes and the leakage matrix. The leaks are held fixed during the fit for the target mode. The asymmetry of the line profiles is taken into account by using an asymmetrical profile that is derived by a generalization of the profile of Nigam & Kosovichev (1998). This way undesirable properties of the profile of Nigam & Kosovichev (1998) are avoided, viz. its invalidity far from the mode frequency and the non-boundedness of its integral over all frequencies (Larson & Schou 2015).

In the following we will use the term "JS" when we are referring to the mean-multiplet technique.

2.3. *Fitting methodologies of Korzennik*

The high-degree fitting methodology of Korzennik et al. (2004) is applicable to modes with degrees in the range from $l \gtrsim 100$ (p-modes) to $l \gtrsim 200$ (f-modes). Its basic idea consists of correcting for the bias introduced when fitting a ridge of power at high degrees. For this purpose, a detailed model of the underlying modes that contribute to the distribution of power in a ridge was developed to generate synthetic ridges, which are then fitted using the same methodology employed to fit the observations. Hence, the results of fitting these synthetic data allow the user to derive a measure of the bias between the ridge properties and those of the underlying targeted mode used in the modeling. By means of this measure the results from fitting an observed ridge can be corrected to derive the unbiased properties of the underlying targeted mode.

In the following we will use the term "SKh" when we are referring to the high-degree fitting methodology of Korzennik.

In Korzennik (2005, 2008a,b) a separate medium-degree fitting method has been developed which is applicable to modes with degrees in the range $0 \leq l \leq 300$, and has been optimized for very long helioseismic time series. This methodology includes an optimal sine multi-taper spectral estimator, the complete leakage matrix, i.e. horizontal as well as vertical components, the asymmetric profile of Nigam & Kosovichev (1998), and the simultaneous fitting of individual profiles at all the azimuthal orders m of a given multiplet (n, l). The contamination by nearby modes

(n', l') within the fitting range is also included. Since simultaneous fitting of these contaminants is impractical, the fitting procedure is iterated, i.e. the characteristics of the contaminants used in the fitting correspond to the values fitted at the previous iteration. The leakage matrix coefficients are corrected for the distortion caused by the solar differential rotation, following the formalism of Woodard (1989). The differential rotation is characterized by the expansion coefficients $B_2 = -0.07712$ and $B_4 = -0.04396$ nHz (Korzennik 2023).

In the following we will use the term "SKm" when we are referring to the medium-degree fitting methodology of Korzennik.

2.4. Fitting methodology of the Birmingham Solar Oscillations Network group

The fitting methodology of the Birmingham Solar Oscillations Network (BiSON) group is applicable to low-degree modes with degrees in the range from $0 \leq l \leq 3$, and is described in detail in Broomhall et al. (2009), Davies et al. (2014), and Hale et al. (2016).

The BiSON network comprises six semi-automated solar observing stations that are dedicated to the collection of low-degree (Sun-as-a-star) helioseismic data (Hale et al. 2016). The stations are situated at various sites around the world in order to provide as continuous observations as possible. At each of the six stations, a resonance scattering spectrometer is used to measure the Doppler velocity shift of the 770-nm D1 potassium absorption line by comparing the Doppler shifted potassium absorption line to a reference line in the laboratory frame. These shifts are measured as variations in resonant scattered intensity which are calibrated into radial velocities each day for each of the six stations. Using these data, a time series is built based on a routine that attempts to maximize the signal-to-noise ratio in the low-frequency region (0.8-1.3 mHz). This time series is then converted to the frequency domain using a fast Fourier transform to generate the frequency power spectrum. Finally, either a maximum-likelihood (Broomhall et al. 2009) or a Markov chain Monte Carlo approach (Davies et al. 2014) is employed to fit an asymmetric Lorentzian profile to the peaks in the frequency power spectrum, the parameters being frequency, amplitude, width, rotational splitting and fractional asymmetry. Howe et al. (2015) have shown that the two approaches produce similar results.

In the following we will use the term "BR" when we are referring to the fitting methodology of the BiSON group.

3. DATA

The data analyzed in this study are based on time series of full-disk dopplergrams, acquired by the HMI on the one hand, and on low-degree Sun-as-a-star observations (i.e., observations where the collected light has been integrated over the entire solar surface) acquired by the ground-based observing stations of the BiSON group (Chaplin et al. 1996), on the other hand.

Using the MPTS method we fitted a 67-day, a 72-day, and a 90-day HMI observing run obtained in 2010 to get the tables MPTS(67d), MPTS(72d), and MPTS(90d), respectively, of fitted mode parameters including frequency, line width, line asymmetry, amplitude, and frequency-splitting coefficients a_1 through a_5.

With regard to the mean-multiplet technique, the standard pipeline at Stanford was applied to get the tables of fitted parameters JS(67d), JS(72d), and JS(90d), respectively.

With regard to the fitting methodologies of Korzennik, the table of fitted parameters, SKh(67d), was downloaded from `lweb.cfa.harvard.edu/~sylvain/research/tables/HiL/HMI/2010/`. For the details of the generation of this table we refer to Korzennik et al. (2013). The table of fitted parameters, SKm(72d), was downloaded from `lweb.cfa.harvard.edu/~sylvain/research/tables/MediumL/`. For the details of the generation of this table we refer to Korzennik (2005, 2008a) and Korzennik (2008b). It bears emphasizing that the MPTS, JS, SKh and SKm methodologies all use exactly the same input timeseries.

Broomhall et al. (2009) published one table of raw, best-fitting BiSON frequencies which they computed from an 8640-day time series that lasted for more than 23 years. They also published two other tables of "corrected" BiSON frequencies which they claimed had been corrected to correspond to both "intermediate" and "quiet-Sun" levels of activity. The corresponding levels of the 10.7-cm radio flux that they used to make these corrected frequency tables were 118 solar flux units (sfu) and 64 sfu, respectively. Here, $1\,\mathrm{sfu} = 10^{-22}\mathrm{Wm}^{-2}\mathrm{Hz}^{-1}$. In order to obtain a table of corrected BiSON frequencies that would correspond to the average level of the 10.7-cm radio flux of 77.207 sfu that, according to Table 1, existed during the 90-day time series of HMI observations from which we generated our table MPTS(90d), we linearly interpolated between the "intermediate" and "quiet-Sun" tables of Broomhall et al. (2009). We will refer to this set of interpolated BiSON frequencies as BR(90d).

More details of the data used in our comparative study are given in Table 1.

Table 1. Data used in comparative study

	starting date	n_d	10.7-cm flux	n-range	l-range	ν-range
MPTS(90d)	2010.04.30	7328	77.207	$0-30$	$0-1350$	$964.83-4599.74$
MPTS(72d)	2010.04.30	7328	75.471	$0-30$	$0-1350$	$964.81-4599.56$
MPTS(67d)	2010.05.07	6678	74.988	$0-30$	$0-1000$	$964.78-4599.74$
JS(90d)	2010.04.30	2043	77.207	$0-27$	$0-299$	$954.33-4475.54$
JS(72d)	2010.04.30	1983	75.471	$0-29$	$0-299$	$938.39-4621.47$
JS(67d)	2010.05.07	1984	74.988	$0-28$	$0-299$	$975.17-4482.30$
SKm(72d)	2010.04.30	2322	75.471	$0-30$	$0-300$	$882.98-4527.89$
SKh(67d)	2010.05.07	5714	74.988	$0-14$	$100-1000$	$1421.56-5504.08$
BR(90d)	2010.04.30	79	77.207	$6-28$	$0-3$	$972.61-3984.29$

Note— The numbers in parentheses in column 1 refer to the durations of the observing runs in days analyzed with the MPTS, JS, SKm, SKh, and BR fitting methodologies. The starting date is given in the form yyyy.mm.dd. In the column labeled n_d the number of modes is given that are contained in the corresponding frequency table listed in column 1. The 10.7-cm flux is measured in solar flux units (sfu), where $1\,\mathrm{sfu} = 10^{-22}\mathrm{Wm}^{-2}\mathrm{Hz}^{-1}$. As described in the text, the interpolated BiSON frequency table BR(90d) corresponds to a radio flux of 77.207 sfu. The frequency range in column 7 is measured in μHz.

4. INTERCOMPARISON OF FITTED FREQUENCIES

In Table 2 we show the results of our comparison of the JS, SKm, SKh, and BR frequencies with the MPTS frequencies, and the SKm, SKh, and BR frequencies with the JS frequencies.

Table 2. Comparison of the MPTS method with the JS, BR, SKm and SKh methods, and the JS method with the BR, SKm, and SKh methods in terms of raw and normalized frequency differences

difference				raw				normalized				
	n_{d}	$l_{\min}$	$l_{\max}$	ave	std	$|t|$	p	ave	std	$|t|$	p	$n_{\pm 3\,\sigma}$
MPTS(90d)$-$BR(90d)	76	0	3	$+0.006$	0.389	0.144	0.886	-0.077	1.168	0.575	0.567	1
JS(90d)$-$BR(90d)	44	0	3	-0.032	0.151	1.425	0.161	-0.112	1.120	0.661	0.512	0
MPTS(90d)$-$JS(90d)	2042	0	299	$+0.013$	0.185	3.100	0.002	$+0.510$	1.347	17.105	≈ 0	86
MPTS(72d)$-$JS(72d)	1980	0	299	$+0.017$	0.101	7.454	≈ 0	$+0.496$	1.260	17.515	≈ 0	61
MPTS(67d)$-$JS(67d)	1984	0	299	$+0.017$	0.112	6.805	≈ 0	$+0.461$	1.238	16.564	≈ 0	59
MPTS(72d)$-$SKm(72d)	2313	0	300	$+0.026$	0.346	3.683	≈ 0	$+0.555$	1.385	19.283	≈ 0	104
JS(72d)$-$SKm(72d)	1972	0	299	$+0.019$	0.089	9.717	≈ 0	$+0.334$	0.955	15.536	≈ 0	16
JS(67d)$-$SKh(67d)	517	100	299	$+0.009$	1.690	0.116	0.907	$+0.515$	4.223	2.775	0.006	150
MPTS(67d)$-$SKh(67d)	4689	100	1000	$+1.248$	1.211	70.576	≈ 0	$+8.425$	6.618	87.172	≈ 0	3568

NOTE— The differences are in the sense as indicated in the first column. The sample sizes are given in the column labeled n_{d}. In the columns labeled $l_{\min}$ and $l_{\max}$, respectively, the minimum and maximum degree used in each comparison is listed. For both the raw and the normalized frequency differences the average and the standard deviation are listed in the columns labeled ave and std, respectively. The normalizations were carried out by dividing the raw frequency differences $\Delta\nu = \nu_1 - \nu_2$ by the formal error $\sigma_{\Delta\nu} = \sqrt{\sigma_1^2 + \sigma_2^2}$ of each difference, where σ_1 and σ_2 denote the uncertainty of ν_1 and ν_2, respectively. Using Student's t-Test, each mean raw and each mean normalized frequency difference was tested for a significant deviation from zero. The absolute magnitude of the t-value and the probability that the sample difference occurred by chance are listed in the columns labeled $|t|$ and p, respectively. The reason we are showing $|t|$ is because we are employing a two-sided hypothesis test (i.e., $H_0:$ ave $= 0$). Since we are using a two-sided test, it is irrelevant whether ave < 0 or ave > 0. The number of points for which the frequency difference exceeds $3\,\sigma$ in absolute magnitude for each case is listed in the column labeled $n_{\pm 3\,\sigma}$. The raw frequency differences are measured in μHz. The horizontal lines separate the low, medium and high degree comparisons.

The first two rows of Table 2 contain the results of the two comparisons that we made that contained only low-degree $(0 \leq l \leq 3)$ mode frequencies. The first row shows the statistics of the comparison of the MPTS(90d) frequencies with the frequencies of BR(90d). Comparison of the average raw frequency differences shown in column 5 of this table shows that the raw average frequency difference for this case had the smallest absolute value of the nine cases that are shown. Also, the results of Student's t-test for this case showed that the probability that these frequency differences were random events was equal to 0.886. The tiny average size of this set of raw frequency differences is supported by the fact that the corresponding normalized average shown in column 9 was the smallest of those averages. The randomness of these normalized differences is supported by the large probability of 0.567 in column 12. Additionally, only one of the 72 MPTS(90d)$-$BR(90d) frequency differences exceeded $\pm 3\,\sigma$, where $\sigma = \sigma_{\Delta\nu} = \sqrt{\sigma_1^2 + \sigma_2^2}$. Here, σ_1 and σ_2 denote the uncertainty of ν_1 and ν_2, respectively.

The second row of Table 2 shows the statistics of the comparison of the JS(90d) frequencies with the low-degree BR(90d) frequencies. While the average raw frequency difference for this comparison is nearly six times larger in absolute magnitude than the average raw difference of the MPTS(90d)$-$BR(90d) case, the average of the normalized differences was the second-smallest of the nine averages in column 9. Additionally, the application of Student's t-test

Table 3. Comparison of the MPTS method with the JS, BR, SKm and SKh methods, and the JS method with the BR, SKm, and SKh methods in terms of the scaled relative frequency differences

difference	scaled relative			
	ave	std	$|t|$	p
MPTS(90d)−BR(90d)	4.29×10^{-7}	1.01×10^{-4}	0.037	0.971
JS(90d)−BR(90d)	-7.55×10^{-6}	4.75×10^{-5}	1.056	0.297
MPTS(90d)−JS(90d)	2.37×10^{-6}	4.55×10^{-5}	2.356	0.019
MPTS(72d)−JS(72d)	3.58×10^{-6}	2.37×10^{-5}	6.704	≈ 0
MPTS(67d)−JS(67d)	3.67×10^{-6}	2.61×10^{-5}	6.261	≈ 0
MPTS(72d)−SKm(72d)	4.66×10^{-6}	9.94×10^{-5}	2.253	0.024
JS(72d)−SKm(72d)	4.38×10^{-6}	2.19×10^{-5}	8.867	≈ 0
JS(67d)−SKh(67d)	-1.49×10^{-5}	3.87×10^{-4}	0.878	0.380
MPTS(67d)−SKh(67d)	9.16×10^{-5}	1.52×10^{-4}	41.359	≈ 0

NOTE— The differences are in the sense as indicated in the first column. The scaling of the relative frequency differences, $\Delta\nu/\nu = (\nu_1 - \nu_2)/[(\nu_1 + \nu_2)/2]$, was carried out by multiplying each difference with a factor Q, where Q is the ratio of the corresponding mode inertia to that of a mode of degree zero with the same frequency. For the differences the average and the standard deviation are listed in the columns labeled ave and std, respectively. The absolute magnitude of the t-value and the probability that the sample difference occurred by chance are listed in the columns labeled $|t|$ and p, respectively.

to the raw and normalized frequency differences showed that the probabilities they were random events were equal to 0.161 and 0.512, respectively. Furthermore, none of the JS(90d)−BR(90d) differences exceeded $\pm 3\,\sigma$.

Rows 3 through 8 of Table 2 show the results of the six different comparisons of larger tables that contained different combinations of low and medium-degree modes. Rows 3, 4, and 5 show the results of comparisons of the MPTS and JS frequencies that were derived from observational time series that had durations equal to 90, 72, and 67 days, respectively. In contrast to the results shown in rows 1 and 2, the application of Student's t-test for these three cases showed that all three sets of raw frequency differences and all three sets of normalized differences were systematically different from being random events at the level of $0.2\,\%$ or better. We will return to this point in our discussion of Tables 5 and 6. For these same three cases, the average normalized frequency differences were very similar and were all less than $0.40\,\sigma$, while the numbers of cases that exceeded $\pm 3\,\sigma$ were all less than $4.5\,\%$ of the total numbers of cases.

Rows 6 and 7 of Table 2 shows the results of comparing the MPTS(72d) and JS(72d) frequencies with the SKm(72d) frequencies. As with the three previous cases, the application of Student's t-test to the MPTS(72d)−SKm(72d) comparison in row 6 shows that none of the raw or normalized frequency differences were random events. The average of the normalized frequency differences for this case was equal to $0.40\,\sigma$, while the fraction of cases that exceeded $\pm 3\,\sigma$ was equal to $4.49\,\%$.

Row 7 of Table 2 shows the statistics for the JS(72d)−SKm(72d) comparison. Student's t-test shows that neither the raw nor the normalized frequency differences were random events. The average of the normalized frequency differences for this case was equal to $0.35\,\sigma$, while the fraction of cases that exceeded $\pm 3\,\sigma$ was equal to $0.81\,\%$.

Row 8 of Table 2 shows the first of two comparisons with the SKh method, namely the statistics of the JS(67d)−SKh(67d) comparison. The absolute value of the average of these raw frequency differences was the second-smallest of the nine averages in this table. Furthermore, the results of Student's t-test on these raw differences appear to show that those differences were random events; however, as we will describe later when we show the degree dependence of these differences in Figure 8, the small value of the t-statistic is misleading in this case because of the opposite signs of the low- and intermediate-degree frequency differences. Furthermore, the application of Students's t-test to this set of normalized frequency differences shows that they were random events at the level of $0.6\,\%$ Also, row 8 shows that $29.0\,\%$ of the normalized JS(67d)−SKh(67d) differences exceeded $\pm 3\,\sigma$. The comparison of the results in rows 7 and 8 clearly shows that the SKm method is vastly superior to the SKh method for degrees of 299 and below.

Row 9 of Table 2 shows the results of the second of our two comparisons with the SKh method. This row shows the statistics of the MPTS(67d)−SKh(67d) comparison. The average value of these raw frequency differences was 39 times larger in absolute value than the second-largest average that was shown in row 2. Row 9 also shows that both the raw and normalized SKh(67d) frequencies differed systematically from the MPTS(67d) frequencies, with the t-test showing a probability effectively equal to zero of the raw and normalized differences being random. Furthermore, a total of 76.1 % of the normalized differences exceeded $\pm 3\,\sigma$.

Basu et al. (2003) compared tables of frequencies which they generated using both the JS method and the GONG PEAKFIND fitting method on both GONG and MDI time series. Some details of the GONG pipeline algorithm were provided by Anderson et al. (1990). Instead of using $\Delta\nu$, these authors used the scaled relative frequency differences, $Q_{n,l}\Delta\nu_{n,l}/\nu_{n,l}$, where $Q_{n,l}$ is the ratio of the mode inertia $I_{n,l}$ of a mode with degree l and order n to that of a mode of degree zero with the same frequency (Christensen-Dalsgaard & Berthomieu 1991). Even though they found that their average relative errors were typically less than 1×10^{-5}, which they pointed out was substantially smaller than the formal errors in the differences, they also pointed out that some of their frequency differences showed "... a systematic behavior that might nonetheless influence the inversion results."

In order to place the nine different sets of frequency differences that we have shown in Table 2 in the context of the different sets of GONG and MDI frequency differences published by Basu et al. (2003), we employed a table of $Q_{n,l}$ values that extended up to $l = 1350$ and converted our nine sets of raw frequency differences into nine sets of scaled relative frequency differences. As soon as we had finished generating all nine sets of scaled relative frequency differences, we computed the overall averages of them, and we computed the standard deviations about these averages. We show all nine average differences in the second column of Table 3, and we show all nine standard deviations in the third column of this table. In the fourth column, we show the t-statistic for each of these comparisons, and in the fifth column we show the probability that each set of differences was a random occurrence.

Inspection of column two of Table 3 shows that only for the JS(67d)−SKh(67d) andMPTS(67d)−SKh(67d) cases were the average scaled relative frequency differences greater than 10^{-5}. Also, inspection of the probabilities that are listed in column 5 shows that, while the probabilities for both the MPTS(90d)−JS(90d) and MPTS(72d)−SKm(72d) cases were slightly larger than 0, they were both smaller than 0.025, so both of these sets of scaled relative frequency differences were random at the 2.5 % confidence level. Lastly, the probability of 0.380 for the JS(67d)−SKh(67d) case is intermediate between the probabilities of 0.907 and 0.006 for the raw and normalized differences, respectively.

Before we discuss the possible systematic frequency differences in all nine comparisons, we next show the percentages of the normalized frequency differences that are less than or equal to $1\,\sigma$, $2\,\sigma$, and $3\,\sigma$, respectively in Table 4. Only for the MPTS(67d)−SKh(67d) and JS(67d)−SKh(67d) comparisons are there appreciable proportions of differences that exceed $3\,\sigma$.

Table 4. Percentage of normalized frequency differences that are less than or equal to $1\,\sigma$, $2\,\sigma$, and $3\,\sigma$, respectively.

comparison	$1\,\sigma$	$2\,\sigma$	$3\,\sigma$
MPTS(90d)−BR(90d)	67.11	94.74	98.68
JS(90d)−BR(90d)	65.91	93.18	100.00
MPTS(90d)−JS(90d)	55.53	85.26	95.79
MPTS(72d)−JS(72d)	56.16	86.46	96.92
MPTS(67d)−JS(67d)	58.01	87.20	97.03
MPTS(72d)−SKm(72d)	55.86	84.39	95.50
JS(72d)−SKm(72d)	71.55	94.32	99.19
JS(67d)−SKh(67d)	27.85	54.16	70.99
MPTS(67d)−SKh(67d)	8.15	16.19	23.91

Table 5. Number of frequency and degree bins, respectively, where the error bar, which is equal to the standard error of the mean, does cross zero for the comparisons listed in the first column.

comparison	# frequency bins where the error bar does cross zero	# degree bins where the error bar does cross zero
MPTS(90d)−BR(90d)	6 of 11	2 of 4
JS(90d)−BR(90d)	6 of 8	2 of 4
MPTS(90d)−JS(90d)	2 of 14	2 of 11
MPTS(72d)−JS(72d)	2 of 14	1 of 11
MPTS(67d)−JS(67d)	3 of 14	1 of 11
MPTS(72d)−SKm(72d)	4 of 16	2 of 11
JS(72d)−SKm(72d)	0 of 14	1 of 11
JS(67d)−SKh(67d)	0 of 10	3 of 12
MPTS(67d)−SKh(67d)	0 of 14	0 of 16

In addition to computing the average values of the raw frequency differences for all nine cases, we also binned the raw differences as functions of both frequency and degree. Before we describe the lower-row panels in Figures 1 through 9 in which we show these binned values, we first summarize some important statistics about these binned values in Tables 5 and 6. In each row of the second column of Table 5, we show the number of frequency bins for which the average value plus or minus the standard error of the average crosses zero and we also list the total number of frequency bins that were generated. In the same rows of the third column we show the same two quantities for the degree bins. The first two rows of Table 5 contain the results of the two low-degree comparisons that were shown in the first two rows of Table 2. Row 1 shows that over one-half of the binned MPTS(90d)−BR(90d) raw differences as a function of frequency and exactly one-half of the average differences in the degree bins were consistent with zero at the one-sigma level. These results are consistent with the results of Students t-test in row 1 of Table 2, which showed that the un-binned raw frequency differences were statistically random events. As was the case for the MPTS(90d)−BR(90d) comparison, the results shown in row 2 of Table 5 show that the JS(90d)−BR(90d) binned differences were also consistent with zero at the level of one standard error of the mean.

In contrast to these two low-degree comparisons, rows 3 through 8 of Table 5, which include the medium-degree modes, show that the number of binned values that were different from zero at the one-sigma level was a tiny fraction of the total number of either frequency or degree bins. For rows 3 through 7, these results are consistent with the results of Student's t-tests that were shown in Table 2. Only for the JS(67d)−SKh(67d) case shown in row 8 of Table 5 were the binned results inconsistent with the results of Student's t-Test, which indicated that these differences had the highest probability of occurring randomly. We discuss this issue further below. For the MPTS(67d)−SKh(67d) case in row 9 of Table 5, none of the binned values were consistent with zero at the level of one standard error of the mean.

In columns 2 and 3 of Table 6 we show the minimum and maximum, respectively, of the average values within all of the $250\,\mu$Hz wide frequency bins for each of our nine comparisons. In column 4 we show the differences between the maximum and minimum average values. These differences illustrate the peak-to-peak differences in the binned values as functions of frequency. In columns 5 and 6 we show the minimum and maximum values, respectively, of the average values within the bins as functions of degree. In column 7 we show the differences between the maximum and minimum average values in the degree bins. By comparing the nine pairs of differences in columns 4 and 7, we can quickly see that, with the exception of the JS(67d)−SKh(67d) comparison shown in row 8, the binned values have significantly more spread when binned as a function of frequency than as a function of degree. In fact, the ratios of the values in column 4 divided by the values in column 7 range between 1.6 for row 2 and 7.5 for row 5. Taken

₂₉₆ together, the above results suggest that the comparisons that do result in systematic differences are more significant
₂₉₇ when binned as a function of frequency rather than degree.

Table 6.   Minimum, maximum, and maximum minus minimum values of the averages of the frequency differences, measured in μHz, in the frequency and degree bins, respectively, for the comparisons listed in the first column.

comparison	vs. frequency			vs. degree		
	min	max	max−min	min	max	max−min
MPTS(90d)−BR(90d)	−0.099	0.260	0.359	−0.117	0.061	0.178
JS(90d)−BR(90d)	−0.160	0.037	0.197	−0.109	0.018	0.127
MPTS(90d)−JS(90d)	−0.177	0.081	0.258	−0.005	0.031	0.036
MPTS(72d)−JS(72d)	−0.115	0.036	0.148	+0.004	0.028	0.024
MPTS(67d)−JS(67d)	−0.116	0.064	0.180	+0.005	0.029	0.024
MPTS(72d)−SKm(72d)	−0.370	0.055	0.425	−0.014	0.082	0.096
JS(72d)−SKm(72d)	−0.172	0.061	0.233	−0.010	0.050	0.060
JS(67d)−SKh(67d)	−1.907	0.614	2.521	−2.068	0.442	2.510
MPTS(67d)−SKh(67d)	−1.904	2.518	4.422	+0.485	2.536	2.051

₂₉₈   The second significant fact that can be seen in Table 6 is that the spreads in both columns 4 and 7 are all smaller than
₂₉₉ 0.43 μHz for all of the comparisons which do not involve the SKh(67d) table, while the spreads for the comparisons
₃₀₀ that do involve those frequencies range between six and 14 times larger than the largest of the other six spreads in
₃₀₁ each of columns 4 and 7; and the comparisons that also involve those frequencies in row 9 range between 10 and 11
₃₀₂ times larger than the largest of the other six spreads in each of columns 4 and 7. These comparisons make it very
₃₀₃ clear that the one table of frequencies which differs the most from the other eight tables is the SKh(67d) table.
₃₀₄   In Figures 1 through 9, we show the results of our nine different frequency set comparisons in the same order that
₃₀₅ we used in Tables 2 through 6. In these figures we show the frequency dependence of all nine sets of raw frequency
₃₀₆ differences in the upper left-hand panels and we show the frequency dependence of the nine sets of normalized differences
₃₀₇ in the upper-right panels. The upper-left panels are displayed with different y-axis scales in order to include all of
₃₀₈ the outlying cases. In contrast, the upper-right panels are all plotted to a common y-axis scale for easier comparison.
₃₀₉ Also shown in these panels are the $\pm 3\,\sigma$ values for comparison. Because of the tiny sizes of most of the raw frequency
₃₁₀ differences and the differing results of Student's t-Test, we have also binned the raw frequency differences as functions
₃₁₁ of both frequency (shown in the lower-left panels) and degree (shown in the lower-right panels) in order to allow us to
₃₁₂ demonstrate the existence of any systematic effects. All nine pairs of the lower-row panels are plotted using a common
₃₁₃ y-axis scale for easier comparison.
₃₁₄   The upper-left and upper-right panels of Figure 1 show the frequency dependence of the raw and normalized
₃₁₅ MPTS(90d)−BR(90d) frequency differences, respectively. The lower-left panel shows the result of binning the raw
₃₁₆ frequency differences as a function of frequency, while the lower-right panel shows the result of binning the raw fre-
₃₁₇ quency differences as a function of the degree, l, instead. In both of these panels the error bars that are shown are
₃₁₈ the standard errors of the mean values. The upper panels in this figure confirm the results that we presented in row 1
₃₁₉ of Table 2. Specifically, the upper-left panel shows that the raw differences were very small for frequencies below
₃₂₀ 3700 μHz. The same panel also confirms the results that were shown in row 1 of Table 2 where Students t-test showed
₃₂₁ that the raw MPTS(90d)−BR(90d) differences were not systematic but were instead random with a probability of
₃₂₂ 88.6 %. The upper-right panel confirms that only a single one of the normalized MPTS(90d)−BR(90d) frequency
₃₂₃ differences fell outside the $\pm 3\,\sigma$ limits. The lower-left panel shows that the only binned value that exceeded $\pm 0.10\,\mu$Hz
₃₂₄ was the bin centered at 3875 μHz. This result is consistent with the frequency-dependent increase in the scatter of the

raw MPTS(90d)−BR(90d) frequency differences that can be seen in the upper-left panel. The lower-right panel shows that there was not any systematic variation in the raw frequency differences as a function of the degree of the modes.
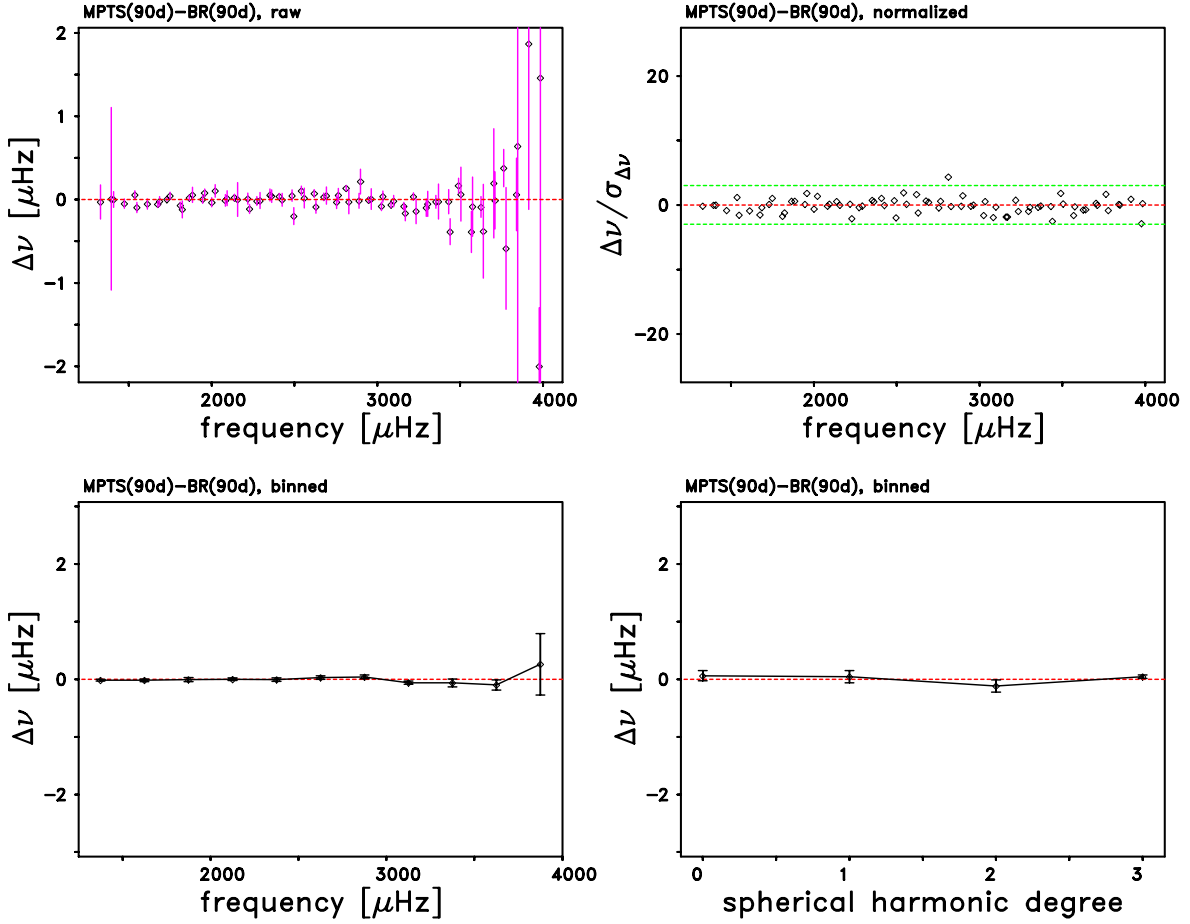

Figure 1.   (Upper-left panel) Raw differences, $\Delta\nu = \nu_{\mathrm{MPTS(90d)}} - \nu_{\mathrm{BR(90d)}}$, as functions of frequency. For some selected differences the error bar is shown in magenta. Here, the error bars are the formal errors of the differences, $\sigma_{\Delta\nu} = \sqrt{\sigma_1^2 + \sigma_2^2}$, where σ_1 and σ_2 denote the uncertainty of $\nu_{\mathrm{MPTS(90d)}}$ and $\nu_{\mathrm{BR(90d)}}$, respectively. (Upper-right panel) Normalized differences, $\Delta\nu/\sigma_{\Delta\nu}$, of the frequencies, as functions of frequency. The normalizaton was carried out by dividing the raw differences $\Delta\nu$ by $\sigma_{\Delta\nu}$. The dashed green lines show the $\pm 3\,\sigma$ values. (Lower-left panel) Binned frequency differences versus frequency using $250\,\mu$Hz-wide bins. Here, the error bars are the standard errors of the means. (Lower-right panel) Binned frequency differences versus degree using 1-degree wide bins. Again, the error bars are the standard errors of the means. In all four panels the dashed red line is for a difference of zero. The y-axis scales of the upper-right and two lower panels have been chosen to be common to Figures 1 through 9.

The four panels of Figure 2 show the JS(90d)−BR(90d) comparison. While the upper-left panel of this figure appears to show a frequency-dependent trend in the raw JS(90d)−BR(90d) differences, this apparent trend is not borne out in either the upper-right panel where the normalized differences are shown as a function of frequency or in the lower-left panel where the binned raw differences are shown. While the lower-right panel of Figure 1 did not show any degree dependence in the binned MPTS(90d)−BR(90d) differences, the lower-right panel of Figure 2 appears to show a very weak variation with degree of the binned JS(90d)−BR(90d) differences.
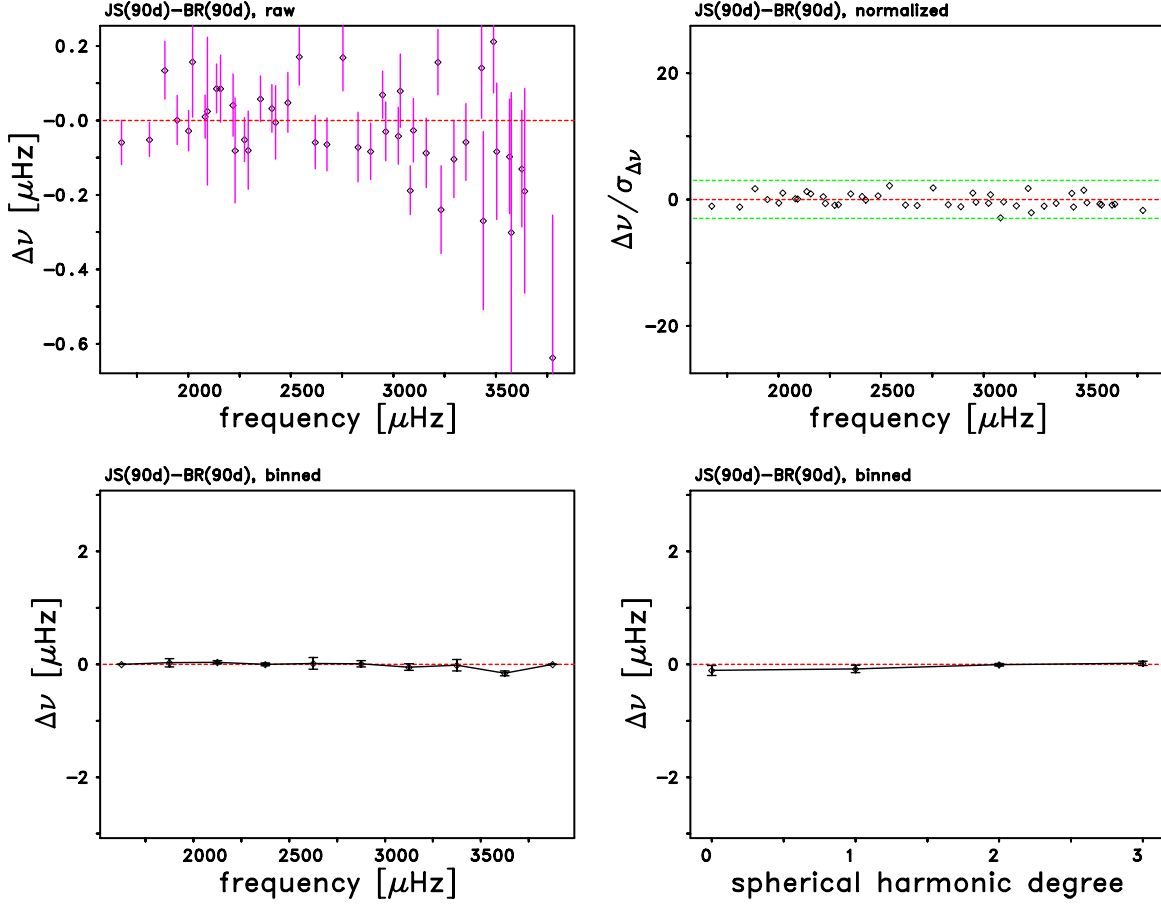
Figure 2. Same as Figure 1, except that the differences, $\Delta\nu = \nu_{JS(90d)} - \nu_{BR(90d)}$, are shown and a different vertical scale is used in the upper-left panel.

The upper-left panel of Figure 3 shows clearly that the scatter in the raw MPTS(90d)−JS(90d) frequency differences increased with increasing frequency. By contrast, the upper-right panel of this figure shows that the normalized frequency differences did not share this tendency and in fact decreased in absolute magnitude at the highest frequencies in the panel. The reason for this different behavior is the fact that the formal frequency uncertainties, which are employed to normalize the raw frequency differences, also increase with increasing frequency. We note that the overall average of these raw differences was shown to be equal to $+0.013\,\mu$Hz in row 3 of Table 2, while the overall average of the normalized differences was equal to $+0.510$. Close inspection of both of the upper panels in Figure 3 shows that there were more negative than positive differences in both cases.
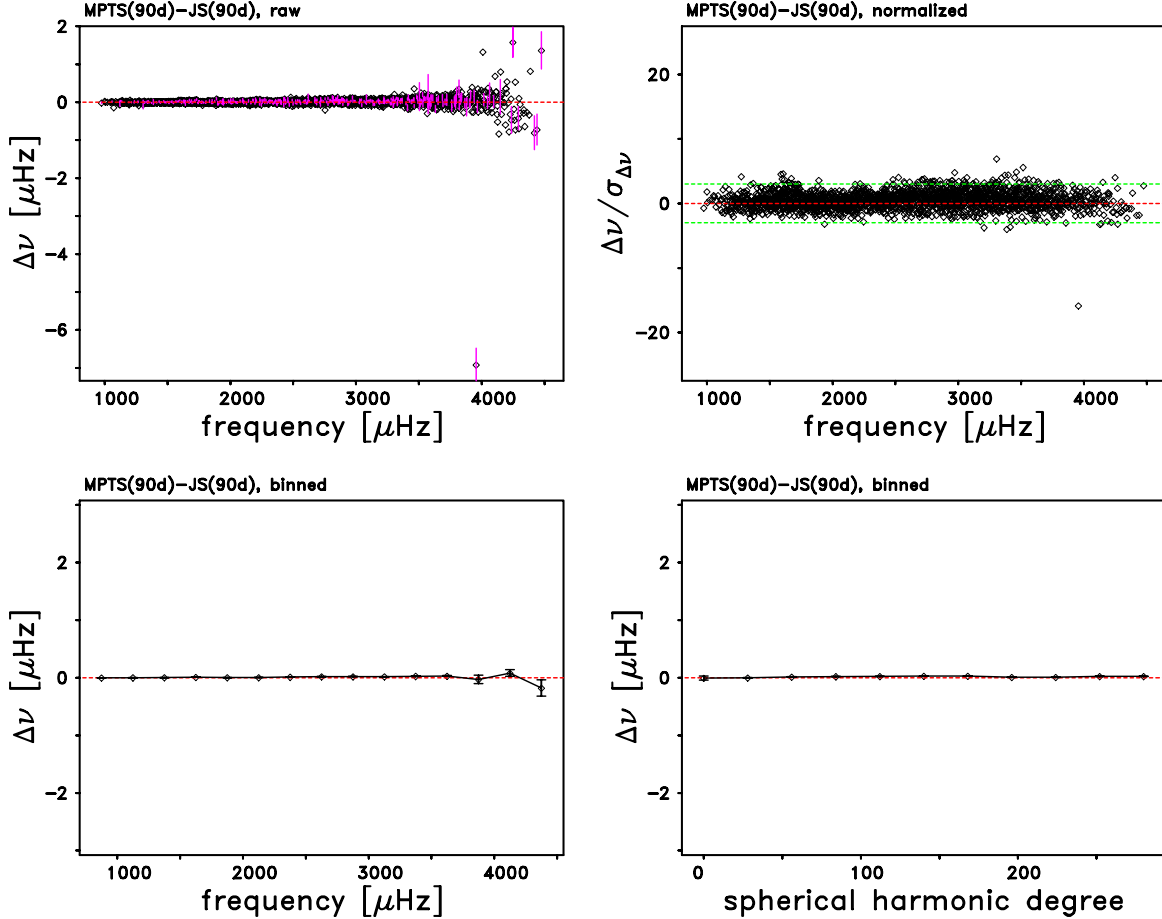
Figure 3. Same as Figure 1, except that the differences, $\Delta\nu = \nu_{\mathrm{MPTS(90d)}} - \nu_{\mathrm{JS(90d)}}$, are shown and a different vertical scale is used in the upper-left panel. In the lower-right panel 28-degree wide bins were used. The rather large outlier near $4000\,\mu$Hz in the upper-left panel is caused by a poor fit of the $(l = 4/n = 26)$ mode by the MPTS method.

In our earlier discussion of the raw MPTS(90d)−JS(90d) differences we noted that the application of Student's t-Test showed that these differences were statistically significant at the 99.8 % level. While the y-axis scale used in both of the lower-row panels in Figure 3 is too large to separate the binned differences and their standard errors clearly from the line showing the zero level, in fact 12 of the 14 binned differences in the lower-left panel were positive, while only two of the three highest frequency averages were negative. Similarly, when we binned the raw differences as a function of degree as shown in the lower-right panel, we found that nine of the 11 averages were positive. Taken together, all four panels of Figure 3 show that the JS(90d) frequencies were systematically smaller than the MPTS(90d) frequencies, but only by tiny fractions of a μHz.

Figure 4 shows the results of the MPTS(72d)−JS(72d) comparison. The four panels of this Figure are nearly identical (after allowing for the different vertical scales in the upper-left panels) to the corresponding panels of Figure 3. This similarity was to be expected based upon the similarity of the results we showed in rows 3 and 4 of Tables 2, 5, and 6.
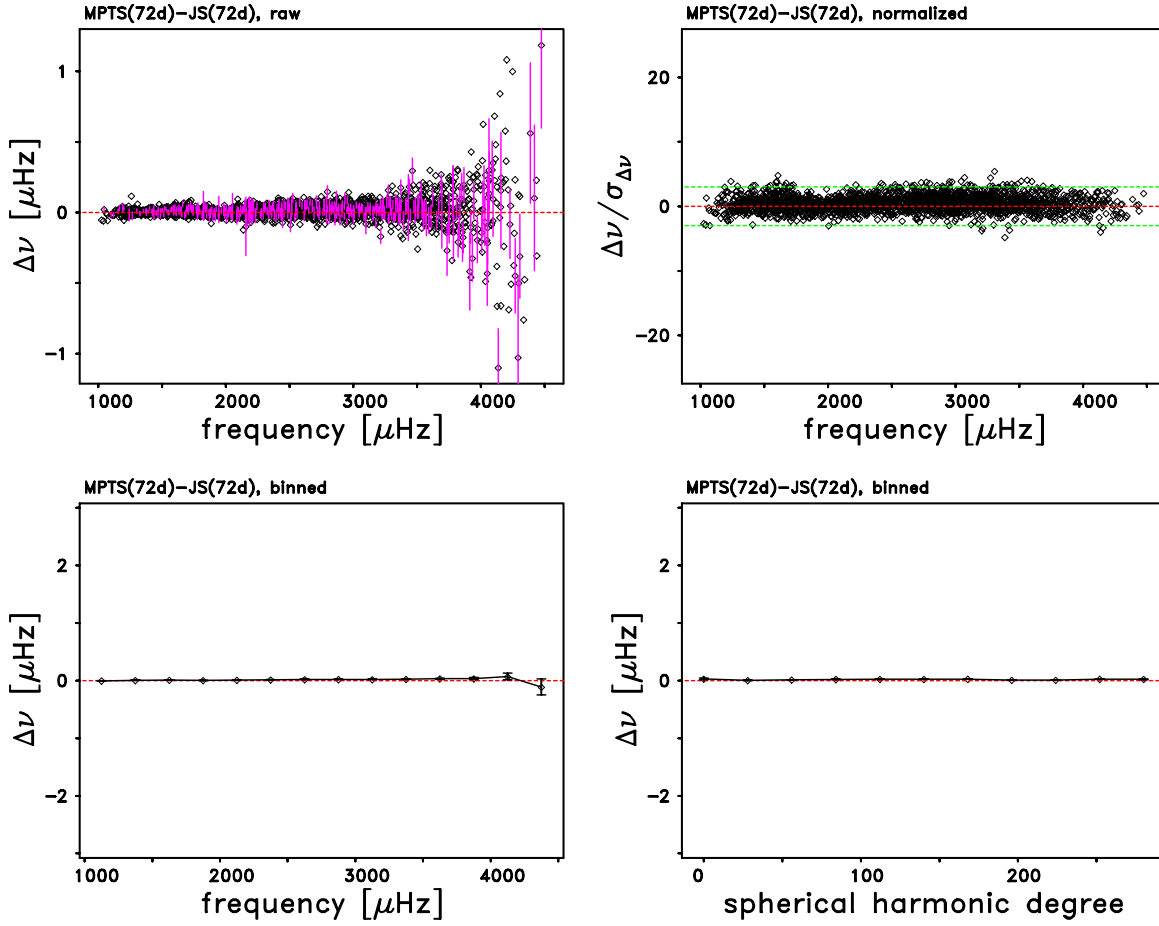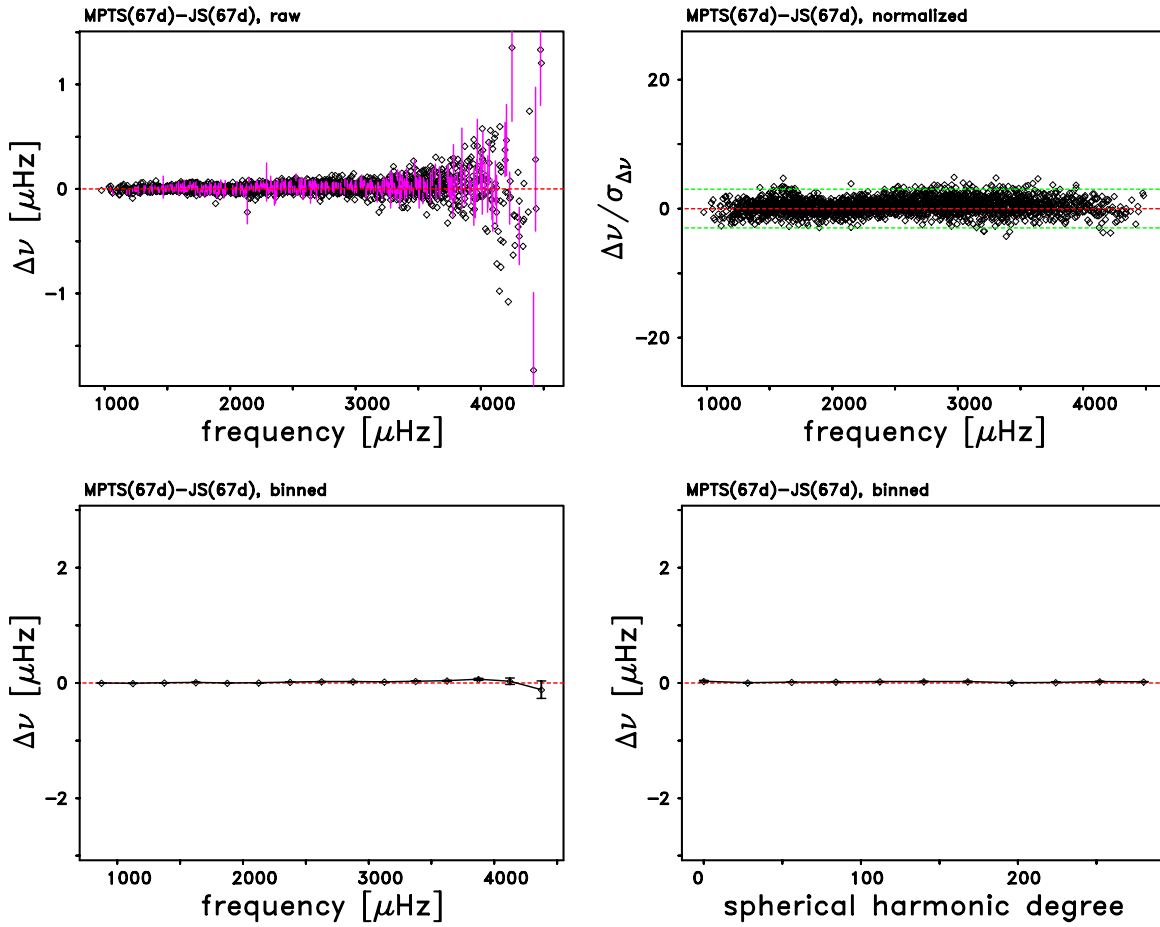

Figure 4. Same as Figure 1, except that the differences, $\Delta\nu = \nu_{\mathrm{MPTS(72d)}} - \nu_{\mathrm{JS(72d)}}$, are shown and a different vertical scale is used in the upper-left panel. In the lower-right panel 28-degree wide bins were used.

Figure 5 shows the results of the MPTS(67d)−JS(67d) comparison. The four panels of this Figure are nearly identical (after allowing for the different vertical scales in the upper-left panels) to the corresponding panels of Figures 3 and 4. These similarities were also to be expected based upon the similarity of the results we showed in rows 3, 4, and 5 of Tables 2, 5, and 6.

Figure 5. Same as Figure 1, except that the differences, $\Delta\nu = \nu_{\mathrm{MPTS(67d)}} - \nu_{\mathrm{JS(67d)}}$, are shown and a different vertical scale is used in the upper-left panel. In the lower-right panel 28-degree wide bins were used.

Figure 6 shows the results of the MPTS(72d)−SKm(72d) comparison. The two upper-row panels of this figure are very similar (after allowing for the different vertical scales in the upper-left panels) to the corresponding panels of Figures 3, 4, and 5. The major differences between this comparison and the comparisons that were shown in those three figures are the larger values of the binned differences that are shown at the right side of the lower-left panel and the small positive binned values around $l = 175$ in the lower-right panel. Both of these differences can also be seen by comparing the results shown in columns 4 and 7 of row 6 of Table 6 with the corresponding values shown in rows 3, 4, and 5 of that table.
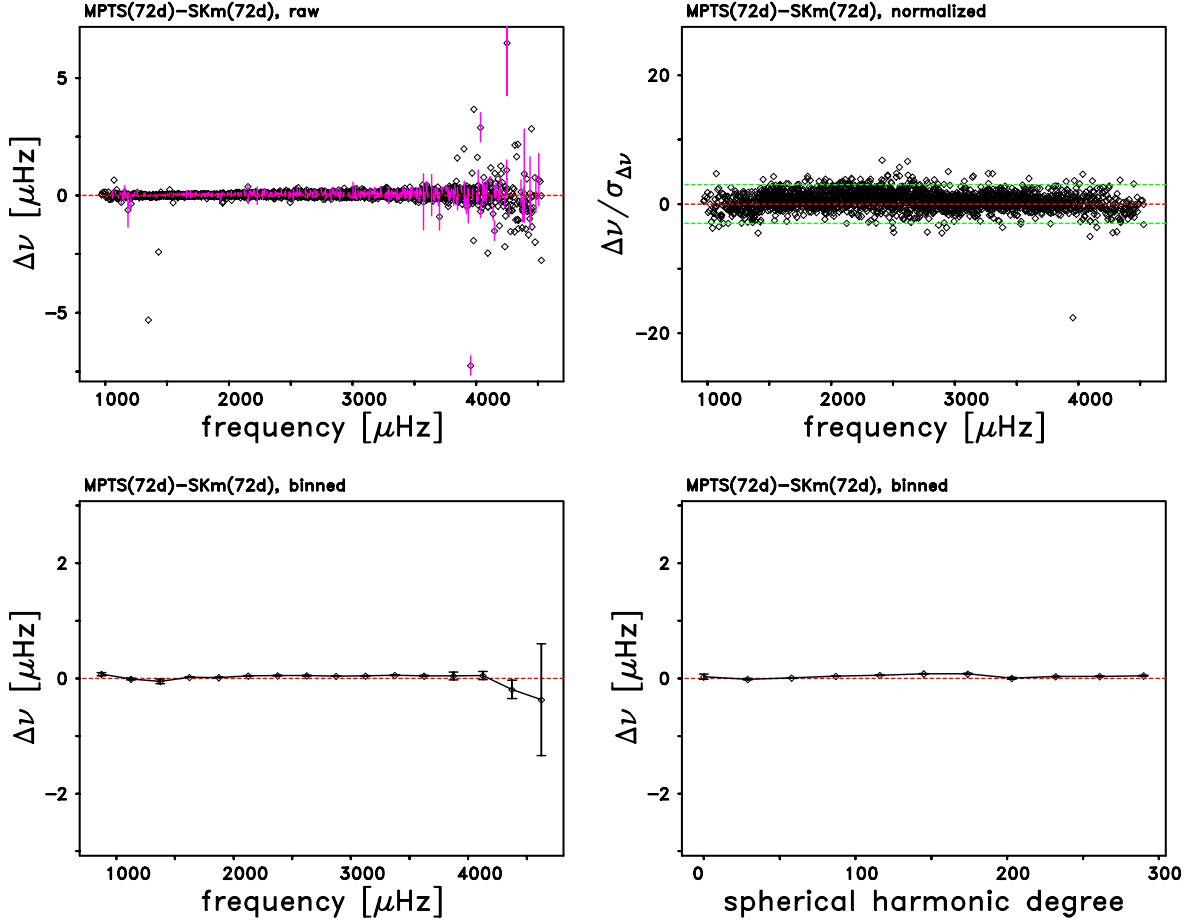
Figure 6. Same as Figure 1, except that the differences, $\Delta\nu = \nu_{\mathrm{MPTS(72d)}} - \nu_{\mathrm{SKm(72d)}}$, are shown and a different vertical scale is used in the upper-left panel. In the lower-right panel 28-degree wide bins were used.

Figure 7 shows the results of the JS(72d)−SKm(72d) comparison. The upper-left panel of this figure is very similar (after allowing for the different vertical scales in the upper-left panels) to the corresponding panels of Figures 3 through 6; however, the upper-right hand panel of this figure shows smaller scatter of the normalized frequency differences than was the case in Figure 6. This difference in the two sets of normalized differences can also be seen by comparing the values in columns nine through 11 in rows six and seven of Table 2. The other differences between this comparison and the (MPTS(72d)−SKm(72d) comparison that we just showed in Figure 6 are the smaller values of the binned differences that are shown at the right side of the lower-left panel and the smaller positive binned values around $l = 175$ in the lower-right panel. Both of these differences can also be seen by comparing the results shown in columns 4 and 7 of row 7 of Table 6 with the corresponding values shown in row 6 of that table.
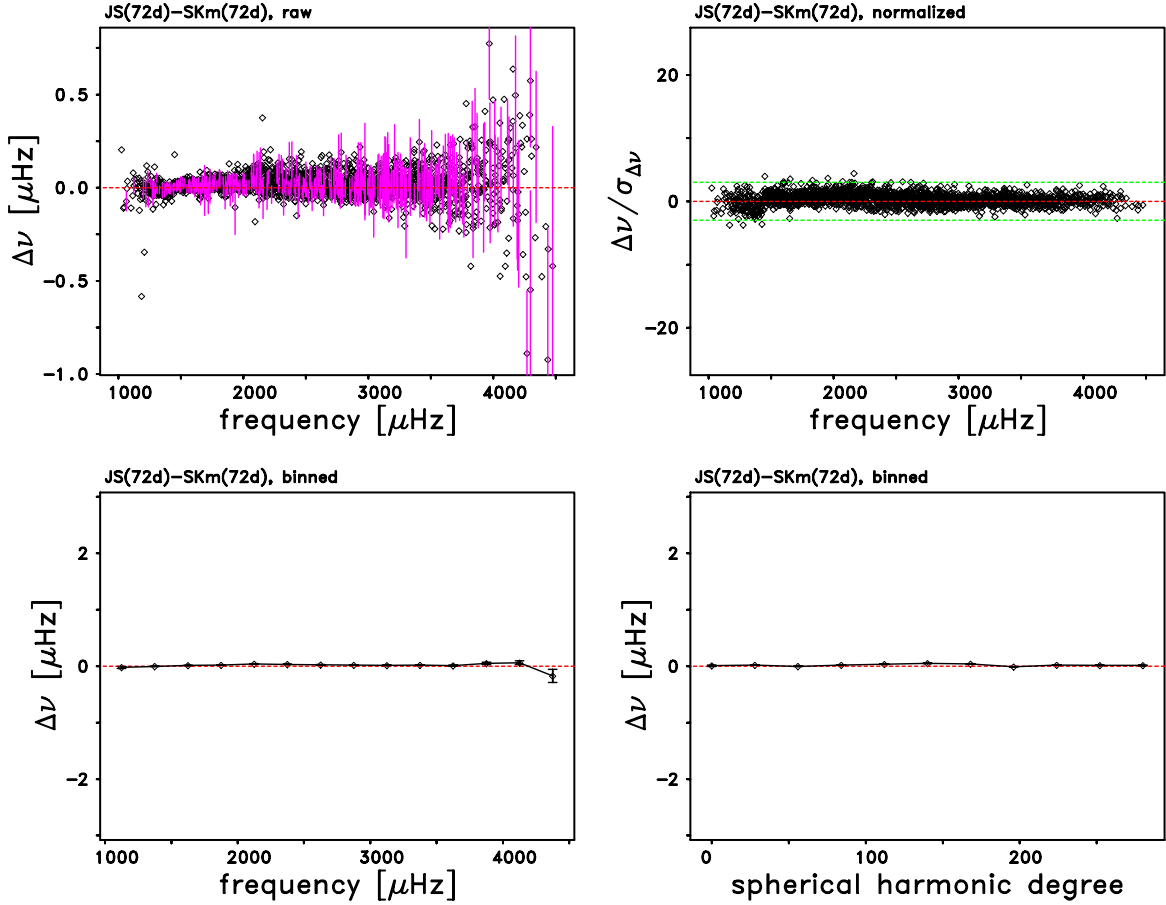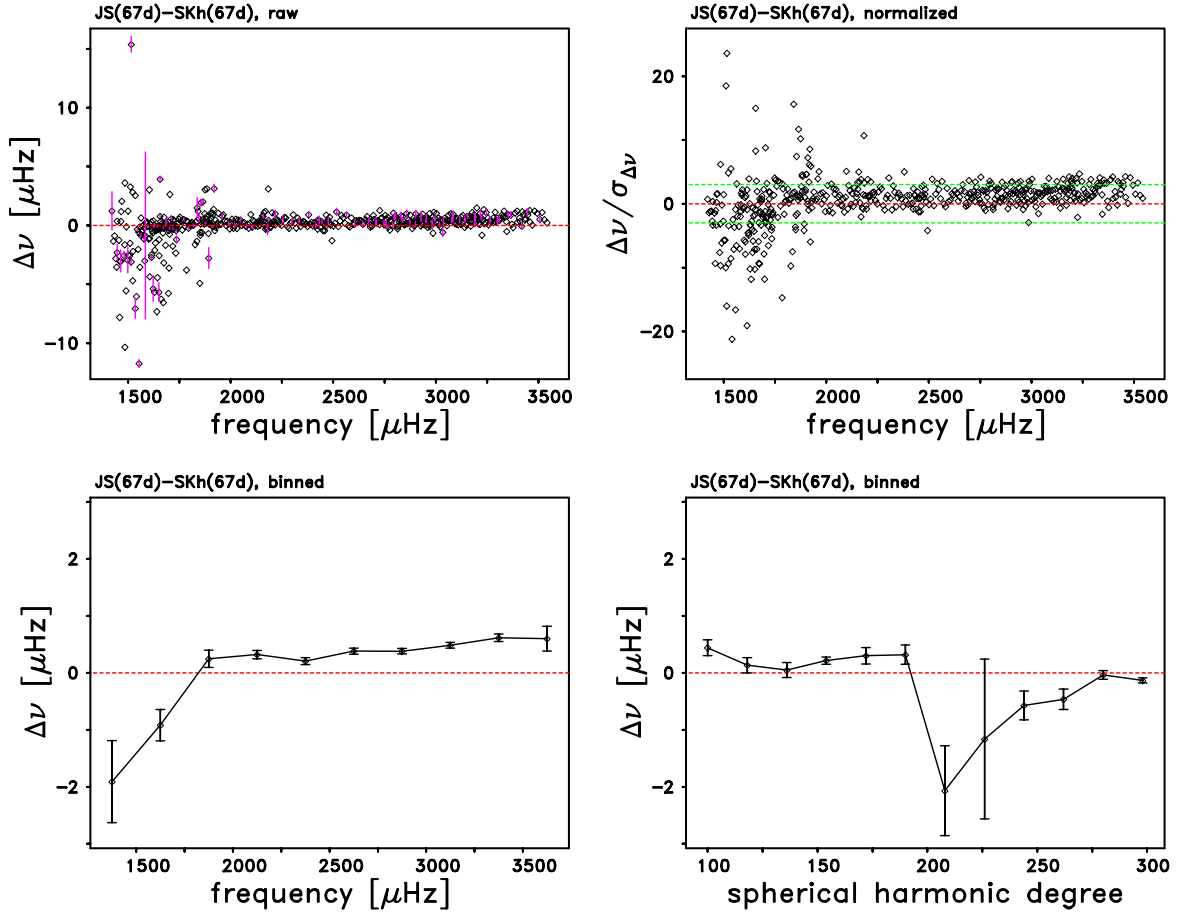

Figure 7. Same as Figure 1, except that the differences, $\Delta\nu = \nu_{\mathrm{JS(72d)}} - \nu_{\mathrm{SKm(72d)}}$, are shown and a different vertical scale is used in the upper-left panel. In the lower-right panel 28-degree wide bins were used.

The four panels of Figure 8 show the JS(67d)−SKh(67d) comparison. While the raw frequency differences are the largest seen yet, they are still smaller than the MPTS(67d)−SKh(67d) differences that we will show in Figure 9. This difference in size of the frequency differences is related to the restricted degree range of the JS(67d)−SKh(67d) comparisons. On the other hand, the frequency dependence of this set of binned frequency differences is qualitatively similar to the pattern shown in the lower-left panel of Figure 9. The lower-right hand panel of Figure 8 shows the difficulty of applying Student's t-Test to two sets of frequencies that have quite different dependence on the degree of the modes. Row 8 of Table 2 claims that there is a probability of 90.7 % that these two tables of frequencies differ randomly. On the other hand, the lower-right panel of Figure 8 shows that this is clearly not the case. The JS(67d)−SKh(67d) frequency differences were all positive for degrees less than 200, while these same differences were all negative for degrees between 200 and 300. These two groups of differences averaged out to yield a very small t-statistic, while in reality these two frequency tables did differ systematically as a function of degree.
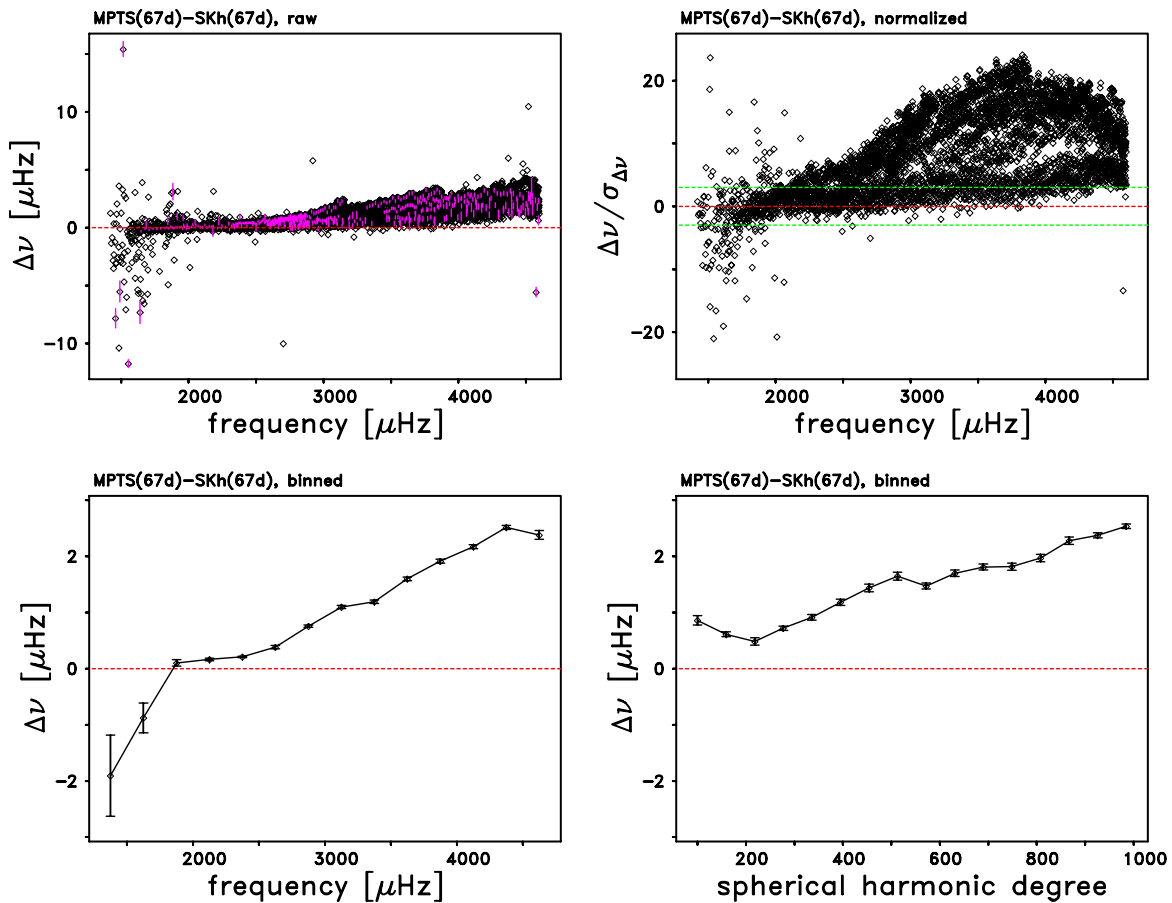

Figure 8. Same as Figure 1, except that the differences, $\Delta\nu = \nu_{\rm JS(67d)} - \nu_{\rm SKh(67d)}$, are shown and a different vertical scale is used in the upper-left panel. In the lower-right panel 18-degree wide bins were used.

The four panels of Figure 9 show the results of the MPTS(67d)−SKh(67d) comparison. In contrast to the tiny differences that were just shown in Figures 1 through 8, all four panels of Figure 9 contain very large differences. In fact, it was the large size of the MPTS(67d)−SKh(67d) frequency differences that led us to adopt a common y-axis scale for the upper-right panels and a different y-axis scale for both lower-row panels in Figures 1 through 9. The two left-hand panels of Figure 9 show a pronounced increase in both the raw and binned MPTS(67d)−SKh(67d) frequency differences as a function of frequency. The upper-right panel shows a slightly different pattern for the normalized MPTS(67d)−SKh(67d) differences. In this panel the differences also grow with increasing frequency but only up to $3800\,\mu$Hz. Above that frequency, the normalized differences decrease slightly in absolute magnitude. The two lower-row panels show that the only differences in the two different sets of binned frequencies occur at the left side of these panels. The low-frequency differences were negative, while the low-degree differences were positive. Otherwise, both sets of binned differences were all strongly positive. The comparison of Figure 9 with Figure 8 shows that, while there are only two methods which fit high-degree power spectra, it is the SKh method which disagrees with both the MPTS method at high degrees and with the JS method at intermediate degrees.

Figure 9. Same as Figure 1, except that the differences, $\Delta\nu = \nu_{\mathrm{MPTS(67d)}} - \nu_{\mathrm{SKh(67d)}}$, are shown and a different vertical scale is used in the upper-left panel. In the lower-right panel 59-degree wide bins were used.

5. DEMONSTRATION THAT DIFFERENCES IN THE SKH(67D) AND MPTS(67D) FREQUENCIES ARE NOT DUE TO THE USE OF INVALID SEED FREQUENCIES IN THE MPTS METHOD

In our comparative study, two methods are included which allow the determination of the high-degree mode parameters, viz. the SKh and the MPTS method. Unfortunately, the multiplet frequencies computed by these two methods disagree clearly, as is shown here in Table 2 and Figure 9, respectively. We wondered if it might be possible to demonstrate that the high-degree frequencies would converge to the MPTS(67d) frequencies if we were to employ the SKh(67d) frequencies in place of our existing seed frequencies as input to the MPTS method. To answer this question

we selected the ridges $n = 0$ through $n = 2$ as test examples. For these ridges it happened that the SKh(67d) and MPTS(67d) a_1 frequency-splitting coefficients differ by not too much for $l > 400$, as is shown here in the left-hand panels of Figures 10, and that the MPTS(67d)−SKh(67d) frequency differences are close to zero around $l \approx 300$, as is shown here in the right-hand panels of Figures 10. While the a_1 frequency-splitting coefficients are crucial for determining the multiplet frequencies, the small frequency differences MPTS(67d)−SKh(67d) around $l \approx 300$ offered us the chance of generating a table of adjusted seed frequencies for the ridges $n = 0$ through $n = 2$ that we could then use in place of our existing seed table for these ridges. In this table of adjusted seed frequencies, $\nu_{\mathrm{seed,adj}}$, we have retained our current seed frequencies for $l \leq 300$ for the $n = 0$ ridge, for $l \leq 260$ for the $n = 1$ ridge, and for $l \leq 200$ for the $n = 2$ ridge, while we have replaced the higher-degree seeds with a set of SKh(67d) frequencies smoothed using high-order Chebyshev polynomials. These thresholds were chosen to make the transition from the original to the adjusted seed frequencies as smooth as possible. Such smooth transitions would not be achievable for ridges of radial order $n > 2$.
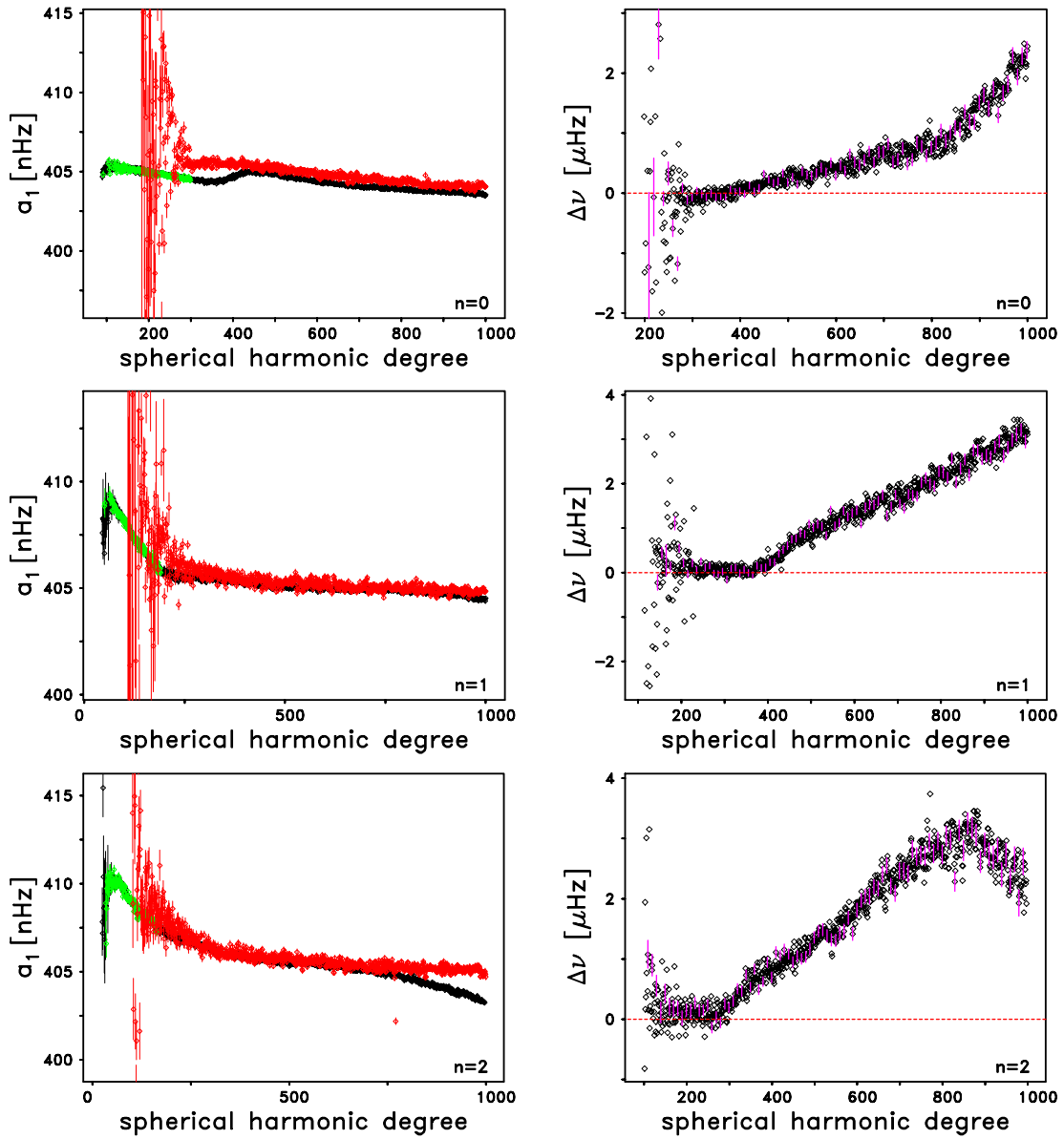
Figure 10. (Left panels) Comparison of the MPTS(67d) (black), JS(67d) (green), and SKh(67d) a_1 frequency-splitting coefficients for, from top to bottom, the ridges $n = 0$ through $n = 2$. (Right panels) Frequency differences $\Delta\nu = \nu_{\mathrm{MPTS}(67d)} - \nu_{\mathrm{SKh}(67d)}$ as functions of the spherical harmonic degree for, from top to bottom, the ridges $n = 0$ through $n = 2$. For some selected differences the error bar is shown in magenta. The error bars are the square root of the sum of the squares of the uncertainties of the two sets of frequencies. The dashed red line is for a difference of zero. Because of the enormous scatter of both the SKh(67d) a_1 frequency-splitting coefficients and the SKh(67d) frequencies for degrees $l < 300$, not all cases are shown at the y-axis scales of the panels.

To ultimately answer the question of whether the high-degree frequencies converge to the MPTS(67d) frequencies by starting with the smoothed SKh(67d) frequencies as the new seed frequencies as input to the MPTS method, we conducted the following multi-iteration scheme, which is known as drawing a homotopy in mathematics. We started the first iteration by fitting the ridges $n = 0$ through $n = 2$ with the MPTS method using the table of adjusted seed frequencies, $\nu_{\text{seed,adj}}$, for these ridges, and left the seeds for the remaining mode parameters (frequency-splitting coefficients, line width, line asymmetry, amplitude) unchanged. The fitted frequencies, $\nu_{\text{fit,iter1}}$, obtained in this way were used as input to the MPTS method in the next iteration, and so on, while the seeds of the remaining mode parameters were left unchanged. In total, we performed 5 such iterations to get the results summarized in the Tables 7 through 9.

In the Tables 7 through 9 we have listed the following four quantities for seven selected modes along, respectively, the ridges $n = 0$ through $n = 2$: 1) the SKh(67d) frequency, ν_{SKh}, 2) the adjusted seed frequency, $\nu_{\text{seed,adj}}$, as derived from ν_{SKh}, 3) the fitted frequency, $\nu_{\text{fit,iter\#}}$, that the MPTS method provided in iteration $\#$ when $\nu_{\text{seed,adj}}$ was used as the seed frequency, and 4) the original MPTS(67d) frequency, ν_{MPTS}. As can be seen, the fitted frequencies approach the original MPTS(67d) frequencies very quickly. This amazingly fast convergence stands in contrast to an experiment conducted by Reiter et al. (2022, in preparation) in which a set of adjusted splitting coefficients were employed that did not contain the large jumps that the MPTS code had converged to for the $n = 0$ ridge when the genuine table of seed coefficients was used as input. In that experiment, Reiter et al. (2022, in preparation) ended up with a set of splitting coefficients that were very close to the original set, but it took a total of 38 iterations.

Table 7. SKh(67d) frequency, ν_{SKh}, adjusted seed frequency, $\nu_{\text{seed,adj}}$, fitted frequency, $\nu_{\text{fit,iter\#}}$, as obtained from the MPTS method in iteration $\#$, MPTS(67d) frequency, ν_{MPTS}, and MPTS(67d) frequency uncertainty, $\sigma_{\nu_{\text{MPTS}}}$, for seven selected modes (l, n) in the degree range from $l = 400$ to $l = 1000$, for the $n = 0$ ridge.

	mode (l, n)						
	$(400,0)$	$(500,0)$	$(600,0)$	$(700,0)$	$(800,0)$	$(900,0)$	$(1000,0)$
ν_{SKh}	2007.9407	2242.1596	2453.6809	2647.7413	2827.6472	2994.9767	3152.5939
$\nu_{\text{seed,adj}}$	2007.86	2242.11	2453.71	2647.72	2827.57	2995.06	3152.70
$\nu_{\text{fit,iter1}}$	2007.9544	2242.3473	2454.1204	2648.3658	2828.3535	2996.5884	3155.1195
$\nu_{\text{fit,iter2}}$	2007.9391	2242.3417	2454.1249	2648.3460	2828.3786	2996.4222	3154.8927
$\nu_{\text{fit,iter3}}$	2007.9373	2242.3514	2454.1220	2648.3900	2828.3485	2996.4214	3154.9244
$\nu_{\text{fit,iter4}}$	2007.9404	2242.3438	2454.1303	2648.4123	2828.3110	2996.6266	3154.9792
$\nu_{\text{fit,iter5}}$	2007.9420	2242.3472	2454.1196	2648.4144	2828.2926	2996.5119	3154.9377
ν_{MPTS}	2007.9402	2242.3497	2454.1274	2648.3965	2828.3849	2996.5227	3155.0457
$\sigma_{\nu_{\text{MPTS}}}$	0.0171	0.0165	0.0187	0.0222	0.0246	0.0295	0.0377

The results presented in Tables 7 through 9 are shown graphically in Figure 11. In the upper-left panel, the frequency changes, $\Delta\nu$, of the frequencies, $\nu_{\text{fit,iter\#}}$, fitted in iteration $\#$ are plotted versus the number of iterations for the 7 modes listed in the Tables 7 through 9 for the $n = 0$ ridge. In order to be able to make the tiny frequency differences visible at all, we have subtracted the SKh(67d) frequency of the mode $(l, n) = (400, 0)$ from all of the five $(400, 0)$ iterated frequencies, and have multiplied the differences by the factor of 100. The remaining six modes $(500, 0), (600, 0) \ldots (1000, 0)$ we treated in the same way. As a result, by definition $\Delta\nu = 0$ for the zeroth iteration for all seven modes. This applies to the ridges $n = 1$ (upper-right panel) and $n = 2$ (bottom panel) as well, because they were processed in exactly the same way. The three panels of Figure 11 clearly show, that the convergence is very fast for all three ridges $n = 0$ through $n = 2$. For all 7 modes considered, after just two to three iterations of the multi-iteration scheme the corresponding original MPTS(67d) frequency has been reached within $\pm 3\,\sigma$.

The convergence behavior of the multi-iteration scheme is analyzed in more detail in Table 10 in terms of the raw frequency differences $\Delta\nu = \nu_{\text{MPTS(67d)}} - \nu_{\text{fit}}$ of the original and the fitted frequencies. Initially, we used the sum

Table 8. Same as Table 7, but for the $n = 1$ ridge.

	mode (l, n)						
	(400,1)	(500,1)	(600,1)	(700,1)	(800,1)	(900,1)	(1000,1)
ν_{SKh}	2555.2422	2800.2943	3030.2041	3249.9327	3462.7476	3670.8995	3875.3840
$\nu_{\mathrm{seed,adj}}$	2555.51	2800.28	3030.11	3249.97	3462.80	3670.68	3875.49
$\nu_{\mathrm{fit,iter1}}$	2555.7776	2801.1451	3031.3602	3251.6104	3464.9073	3673.2826	3878.2637
$\nu_{\mathrm{fit,iter2}}$	2555.7627	2801.2458	3031.4955	3251.6069	3464.8964	3673.5560	3878.5364
$\nu_{\mathrm{fit,iter3}}$	2555.7723	2801.2178	3031.4357	3251.6674	3464.9382	3673.5456	3878.5314
$\nu_{\mathrm{fit,iter4}}$	2555.7699	2801.2288	3031.4477	3251.6653	3464.9225	3673.5643	3878.5483
$\nu_{\mathrm{fit,iter5}}$	2555.7732	2801.2230	3031.4682	3251.6815	3464.9270	3673.5251	3878.5701
ν_{MPTS}	2555.7733	2801.2127	3031.4605	3251.6785	3464.9314	3673.4078	3878.4998
$\sigma_{\nu_{\mathrm{MPTS}}}$	0.0177	0.0192	0.0226	0.0222	0.0476	0.0289	0.0346

Table 9. Same as Table 7, but for the $n = 2$ ridge. Since with the MPTS method only modes with a frequency up to $4600\,\mu$Hz can be fitted, for this ridge the highest degree is $l = 997$.

	mode (l, n)						
	(400,2)	(500,2)	(600,2)	(700,2)	(800,2)	(900,2)	(997,2)
ν_{SKh}	3087.3513	3365.7091	3628.7186	3881.8083	4128.5151	4369.1676	4597.6383
$\nu_{\mathrm{seed,adj}}$	3087.31	3365.59	3628.73	3882.11	4128.47	4369.24	4597.72
$\nu_{\mathrm{fit,iter1}}$	3088.1366	3366.8821	3630.5947	3884.4756	4131.0349	4371.8980	4599.0511
$\nu_{\mathrm{fit,iter2}}$	3088.1392	3366.9045	3630.6265	3884.5033	4131.2427	4372.0325	4599.4037
$\nu_{\mathrm{fit,iter3}}$	3088.1401	3366.9008	3630.6332	3884.5386	4131.2936	4371.9688	4599.4084
$\nu_{\mathrm{fit,iter4}}$	3088.1383	3366.9070	3630.6186	3884.5227	4131.3365	4371.8771	4599.4159
$\nu_{\mathrm{fit,iter5}}$	3088.1372	3366.9013	3630.6226	3884.5324	4131.3668	4371.8577	4599.4070
ν_{MPTS}	3088.1405	3366.9077	3630.6259	3884.5195	4131.3332	4372.0899	4599.5630
$\sigma_{\nu_{\mathrm{MPTS}}}$	0.0246	0.0281	0.0431	0.0295	0.0407	0.0480	0.0678

of squares (SSQ) of the differences, $\Delta\nu$, as a convergence criterion. However, it is an intrinsic feature of the MPTS method that, for a given mode, the iterated frequencies in the multi-iteration scheme scatter on the order of the uncertainty of the fitted mode frequency. As we will demonstrate in the upper-left panels of Figures 12 through 14, the frequency uncertainty increases with increasing full-width at half-maximum (FWHM) line width. Because for high-degree modes the FWHM increases with increasing degree, it is quite clear that in the multi-iteration scheme the scatter of the iterated frequencies increases with increasing degree. As a consequence, the sum of squares turned out to be an unsuitable convergence criterion. Therefore, we switched over to a two-sided Student's t-test, and calculated the probability, p, that the sample differences, $\Delta\nu$, occurred by chance. As can be seen in Table 10, for both ridges $n = 0$ and $n = 1$ this probability, p, exceeds 0.85 already after two to three iterations. However, in terms of p the convergence seems to be much slower for the $n = 2$ ridge.

As mentioned above, in the upper-left panels of Figures 12 through 14 the frequency uncertainties, σ_ν, of the MPTS(67d) frequencies are shown, for the ridges $n = 0$ through $n = 2$, as functions of the MPTS(67d) full-width at half-maximum (FWHM) line widths. In the upper-right panels of these Figures the raw differences, $\Delta\nu = \nu_{\mathrm{MPTS(67d)}} - \nu_{\mathrm{SKh(67d)}}$, of the MPTS(67d) and SKh(67d) frequencies are shown as functions of the MPTS(67d) line widths. Close inspection of the lower two panels in Figure 12 shows that for the first iteration of the frequencies of the $n = 0$ ridge, the scatter increases above a line width of $15\,\mu$Hz, whereas for the fifth iteration of this ridge the transition point is
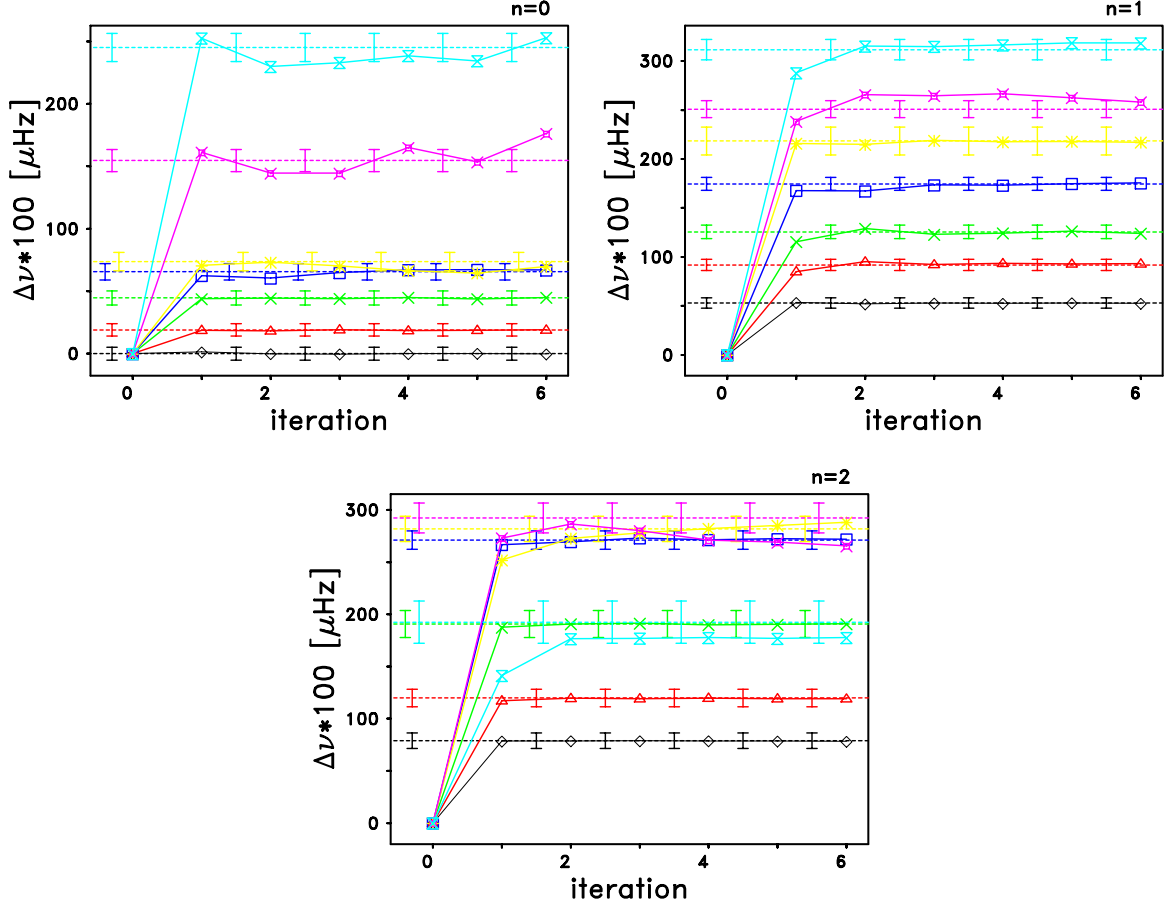
Figure 11. (Upper-left panel) Frequency changes, $\Delta\nu$, of the fitted frequencies, $\nu_{\text{fit,iter\#}}$, in iteration # for the 7 modes listed in Table 7, versus the number of iterations for the $n = 0$ ridge. To be able to adequately represent the tiny frequency differences, the SKh(67d) frequency of the mode $(l, n) = (400, 0)$ was subtracted from all of the five $(400, 0)$ iterated frequencies, and the differences were multiplied by the factor 100. The remaining six modes $(500, 0), (600, 0) \ldots (1000, 0)$ were treated in the same way. As a result, by definition $\Delta\nu = 0$ for iteration #0 for all seven modes. The color style is as follows: $(400/0)$ black, $(500/0)$ red, $(600/0)$ green, $(700/0)$ blue, $(800/0)$ yellow, $(900/0)$ magenta, and $(1000/0)$ turquoise. The colored, dashed horizontal lines with the $\pm 3\,\sigma$ error bars represent the original MPTS(67d) frequencies. The error bars are drawn near the left edge of the panel as well as for the x-values 1.5 through 4.5 in steps of 1.0. (Upper-right panel) Same as upper-left panel, but for the $n = 1$ ridge. (Bottom panel) Same as upper-right panel, but for the $n = 2$ ridge. For this ridge, however, turquoise represents the $(997/2)$ mode.

raised to a width of $30\,\mu$Hz. Similarly, in Figure 13 for the $n = 1$ ridge for the first iteration the transition point occurs for a width of $20\,\mu$Hz, while for the fifth iteration the transition point has been increased to a width of $46\,\mu$Hz. In Figure 14 for the $n = 2$ ridge, there is no such transition point for the first iteration since the raw frequency differences deviate from an average of zero immediately. For the same ridge for the fifth iteration the transition point is located at a width of $50\,\mu$Hz. All three of these changes are clear evidence for the improvements made by the iterative process. The upper-right panels of Figure 12 through 14 show that with the exception of the lowest-degree modes the raw, uniterated frequency differences, $\Delta\nu = \nu_{\text{MPTS(67d)}} - \nu_{\text{SKh(67d)}}$, show tight, systematic variations with increasing linewidth for all three ridges. These tight relationships suggest that one of the two fitting methods becomes less accurate as the line width increases.

Table 10. Convergence of the MPTS method to the original $\nu_{\mathrm{MPTS(67d)}}$ frequencies when the adjusted seed frequencies, $\nu_{\mathrm{seed,adj}}$, were used as input to the MPTS method, for the ridges $n = 0$ through $n = 2$.

	iteration	ave	std	t	p	n_{d}
$n = 0$	0	0.48836	1.26027	10.967	≈ 0	801
	1	0.00613	0.06738	2.745	0.006	911
	2	-0.00023	0.04933	0.140	0.888	911
	3	-0.00026	0.06177	0.126	0.900	911
	4	0.00026	0.07546	0.104	0.917	911
	5	0.00014	0.09464	0.044	0.965	911
$n = 1$	0	1.15403	1.32612	25.888	≈ 0	885
	1	0.03597	0.06851	16.237	≈ 0	956
	2	0.00216	0.03783	1.766	0.078	956
	3	0.00001	0.03736	0.007	0.994	956
	4	0.00021	0.03873	0.170	0.865	956
	5	0.00011	0.04243	0.080	0.936	956
$n = 2$	0	1.53742	1.09960	41.898	≈ 0	898
	1	0.08059	0.12965	19.390	≈ 0	973
	2	0.00952	0.04793	6.195	≈ 0	973
	3	0.00407	0.04389	2.893	0.004	973
	4	0.00287	0.04634	1.932	0.054	973
	5	0.00287	0.05021	1.785	0.075	973

NOTE— After each iteration, as listed in column 2, the average and standard deviation, listed in column 3 and 4, respectively, of the raw differences $\Delta\nu = \nu_{\mathrm{MPTS(67d)}} - \nu_{\mathrm{fit}}$ of the original and the fitted frequencies were calculated. Using the two-sided Student's t-test, these frequency differences were tested for a significant deviation from zero. The t-value and the probability p that the sample difference occurred by chance are listed in the columns labeled t and p, respectively. In the column labeled n_{d} the sample sizes are given. The results given for the zeroth iteration correspond to the results of the raw MPTS(67d)−SKh(67d) frequency differences.
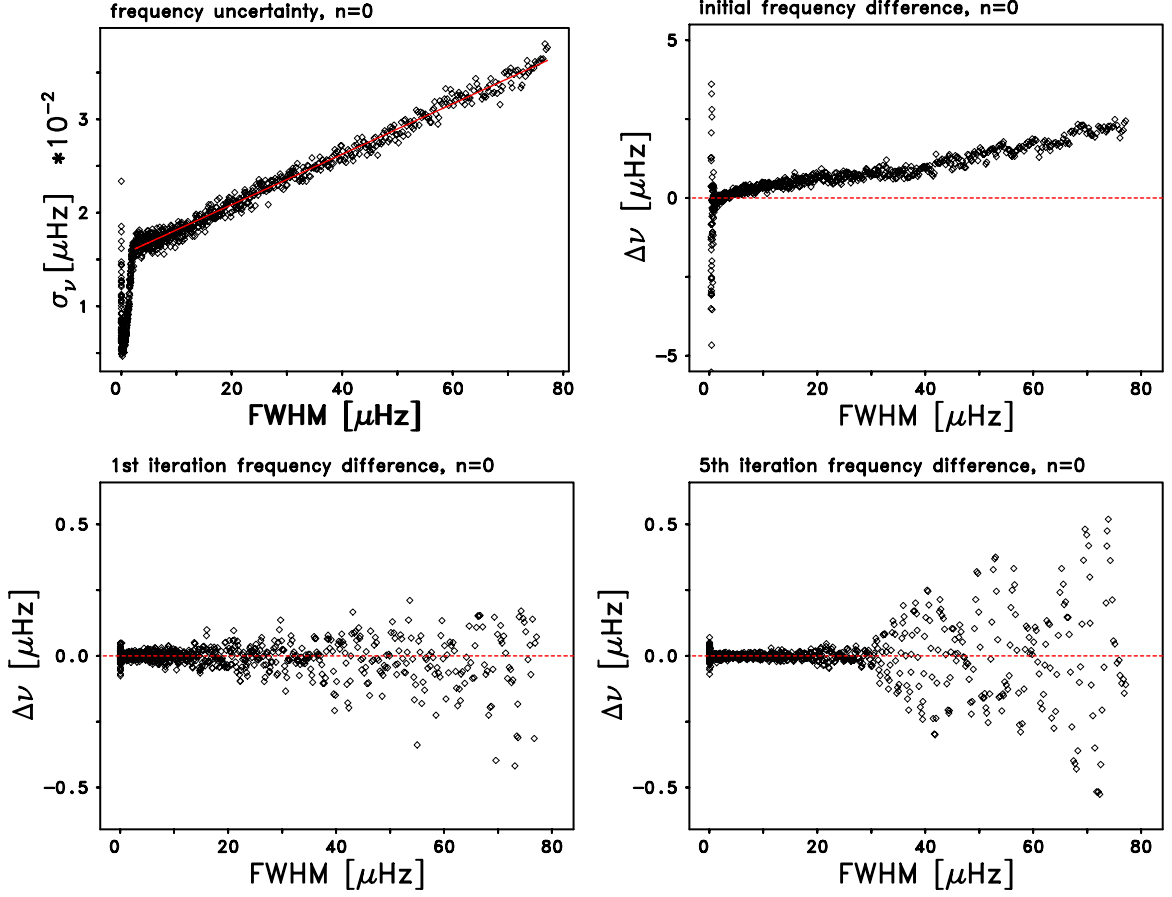
Figure 12. Frequency uncertainties, σ_ν, of the MPTS(67d) frequencies (upper-left panel), raw differences, $\Delta\nu = \nu_{\mathrm{MPTS(67d)}} - \nu_{\mathrm{SKh(67d)}}$, of the MPTS(67d) and SKh(67d) frequencies (upper-right panel), raw differences, $\Delta\nu = \nu_{\mathrm{fit,iter1}} - \nu_{\mathrm{MPTS(67d)}}$, of the $\nu_{\mathrm{fit,iter1}}$ frequencies, as obtained in the 1st iteration and the original $\nu_{\mathrm{MPTS(67d)}}$ frequencies (bottom-left panel), and raw differences, $\Delta\nu = \nu_{\mathrm{fit,iter5}} - \nu_{\mathrm{MPTS(67d)}}$, of the $\nu_{\mathrm{fit,iter5}}$ frequencies, as obtained in the 5th iteration and the original $\nu_{\mathrm{MPTS(67d)}}$ frequencies, as functions of the MPTS(67d) FWHM line width for the $n = 0$ ridge. The full red line in the upper-left panel is for a linear fit for FWHM $\geq 2.5\,\mu$Hz corresponding to the degree $l = 388$. The horizontal dashed red line in the upper-right and the lower panels is for a difference $\Delta\nu = 0$.
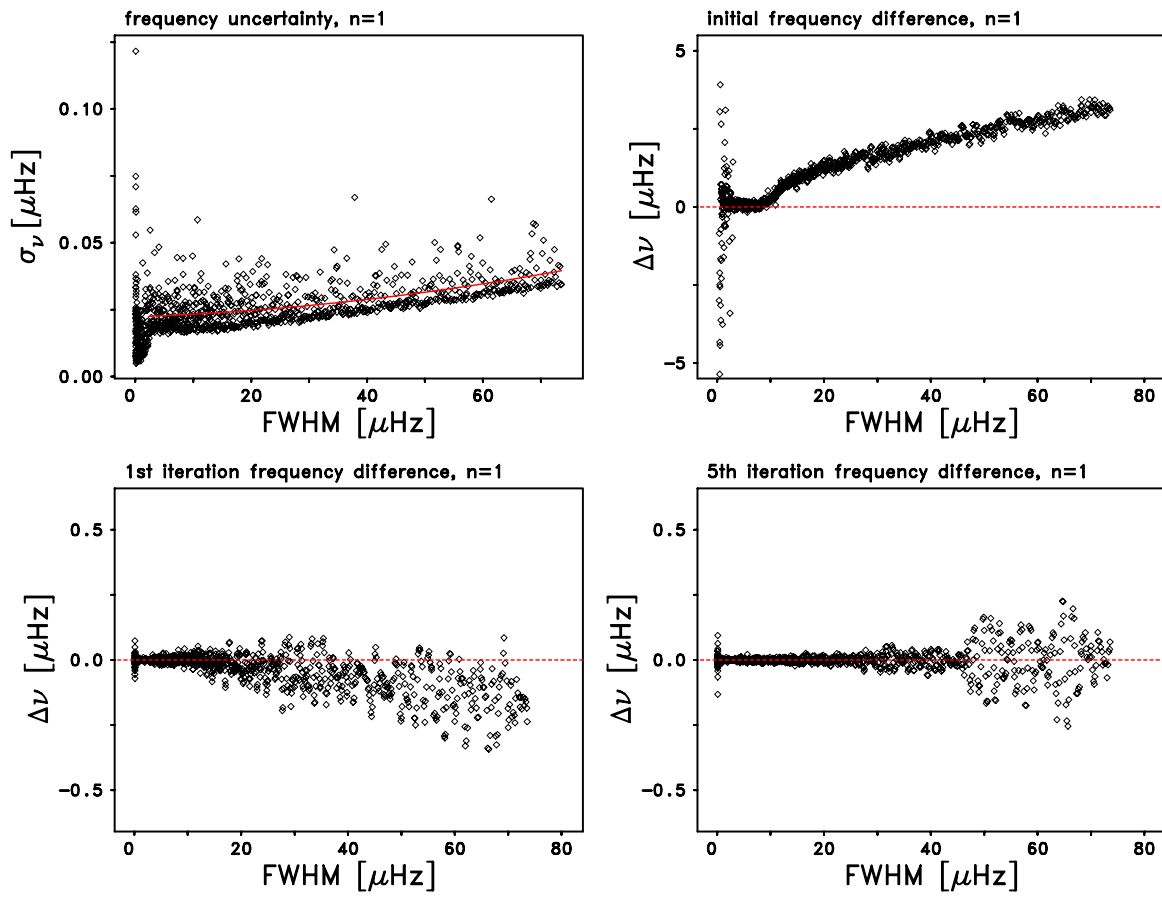
Figure 13. Same as Figure 12, but for the $n = 1$ ridge. The full red line in the upper-left panel is for a parabolic fit for FWHM $\geq 2.5\,\mu$Hz corresponding to the degree $l = 216$.
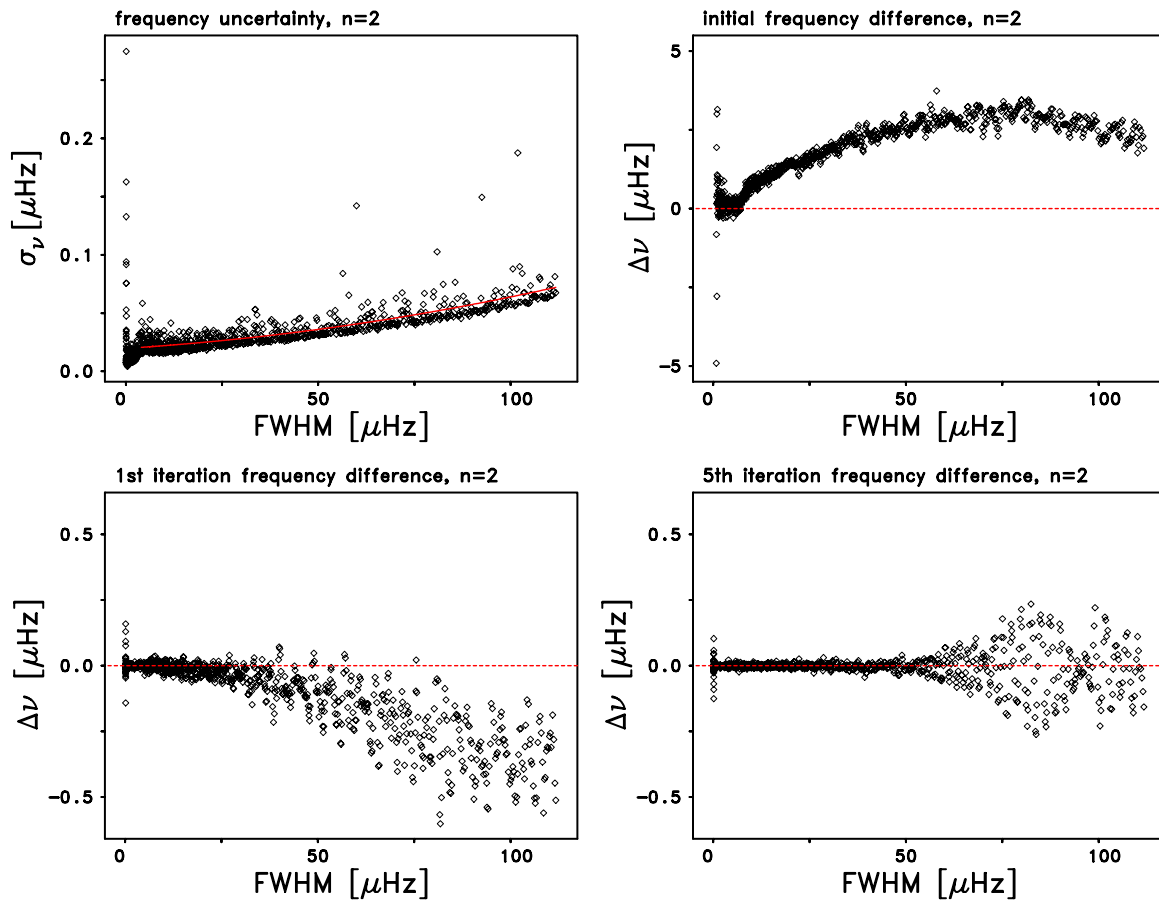
Figure 14. Same as Figure 12, but for the $n = 2$ ridge. The full red line in the upper-left panel is for a parabolic fit for FWHM $\geq 4.0\,\mu$Hz corresponding to the degree $l = 206$.

In the left-hand panel of Figure 15 we show, for the ridges $n = 0$ through $n = 2$, the SKh(67d) full-width at half-maximum (FWHM) line widths, $\mathrm{FWHM_{SKh}}$, plotted as functions of the MPTS(67d) FWHM, $\mathrm{FWHM_{MPTS}}$. It is interesting to note that, for FWHM values above $25\,\mu\mathrm{Hz}$, the slopes of these curves increase as the radial order, n, increases from 0 to 2. In the right-hand panel of Figure 15 we demonstrate how similar the variation of $\sigma_\nu/\mathrm{FWHM_{MPTS}}$ versus $\mathrm{FWHM_{MPTS}}$ is for all three ridges.
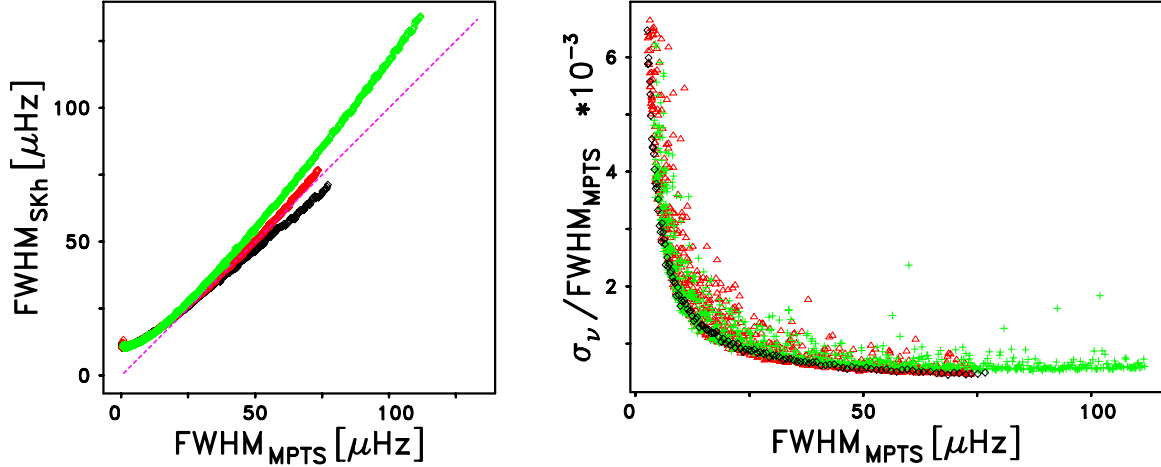
Figure 15. (Left panel) SKh(67d) full-width at half-maximum (FWHM) line widths, $\mathrm{FWHM_{SKh}}$, plotted as functions of the MPTS(67d) FWHM, $\mathrm{FWHM_{MPTS}}$. The black diamonds are for the $n = 0$ ridge, the red triangles are for the $n = 1$ ridge, and the green plus signs are for the $n = 2$ ridge. The dashed magenta line indicates the location for $\mathrm{FWHM_{SKh}} = \mathrm{FWHM_{MPTS}}$. (Right panel) Ratio, $\sigma_\nu/\mathrm{FWHM_{MPTS}}$, of the frequency uncertainties, σ_ν, of the MPTS(67d) frequencies, and $\mathrm{FWHM_{MPTS}}$ plotted as functions of $\mathrm{FWHM_{MPTS}}$. The symbol and color style is the same as in the left-hand panel.

In addition to the frequencies that are produced by a fitting methodology, the formal uncertainties in those frequencies are also of great importance in the generation of structural inversions of the solar interior. Since we have already mentioned that only the MPTS and the SKh methods produce frequencies for the high-degree modes, we have also investigated the frequency uncertainties that are produced by both of these methods. In the three right-hand panels of Figure 16 we present the logarithms of the ratios of the SKh(67d) frequency uncertainties, $\sigma_{\nu,\mathrm{SKh}(67d)}$, to the corresponding MPTS frequency uncertainties, $\sigma_{\nu,\mathrm{MPTS}(67d)}$, as functions of degree, l, for the ridges $n = 0$ through $n = 2$. An overview of these three right-hand panels shows that they share a similar appearance, with the largest ratios clustering at the left side of each panel, and a smaller set of ratios extending from the middle portions to the right sides of the panels. Because of the similarity of the shapes of these three sets of ratios, we chose to divide each set of ratios into two segments, and we then computed the average value of each segment. For the $n = 0$ ridge, the dividing point was located at $l = 375$. The average uncertainty ratio for the modes with lower degrees was 38.7, while the average ratio of the higher-degree cases was 3.9. For both the $n = 1$ and $n = 2$ ridges, the dividing point was located at $l = 275$. For the $n = 1$ ridge, the average of the lower-degree ratios was 19.0, and the average of the higher-degree ratios was 3.8. For the $n = 2$ ridge, the average of the lower-degree ratios was 11.2, and the average of the higher-degree ratios was also equal to 3.8. These statistics make it very clear that the MPTS method produces considerably smaller frequency uncertainties than the SKh method. For the sake of completeness, we show in the three left-hand panels of Figure 16 the logarithms of the ratios of the SKm(72d) frequency uncertainties, $\sigma_{\nu,\mathrm{SKm}(72d)}$, to the corresponding MPTS frequency uncertainties, $\sigma_{\nu,\mathrm{MPTS}(72d)}$, as functions of degree, l, for the ridges $n = 0$ through $n = 2$. Comparison of the pairs of panels in each row of Figure 16 show that the SKm and SKh frequency uncertainties are not self-consistent within each of the three different ranges of overlapping degrees, as the SKm uncertainties are all increasing functions of the spherical harmonic degree, while the SKh uncertainties are all decreasing functions of the spherical harmonic degree. Furthermore, for the $n = 0$ ridge, both the SKm and SKh frequency uncertainties are all larger than the corresponding MPTS uncertainties. Only for the $n = 1$ ridge are some of the SKm uncertainties substantially smaller than the corresponding MPTS uncertainties for degrees below 125. For the $n = 2$ ridge, only about ten of the SKm uncertainties are smaller than the MPTS uncertainties for degrees between 50 and 80.
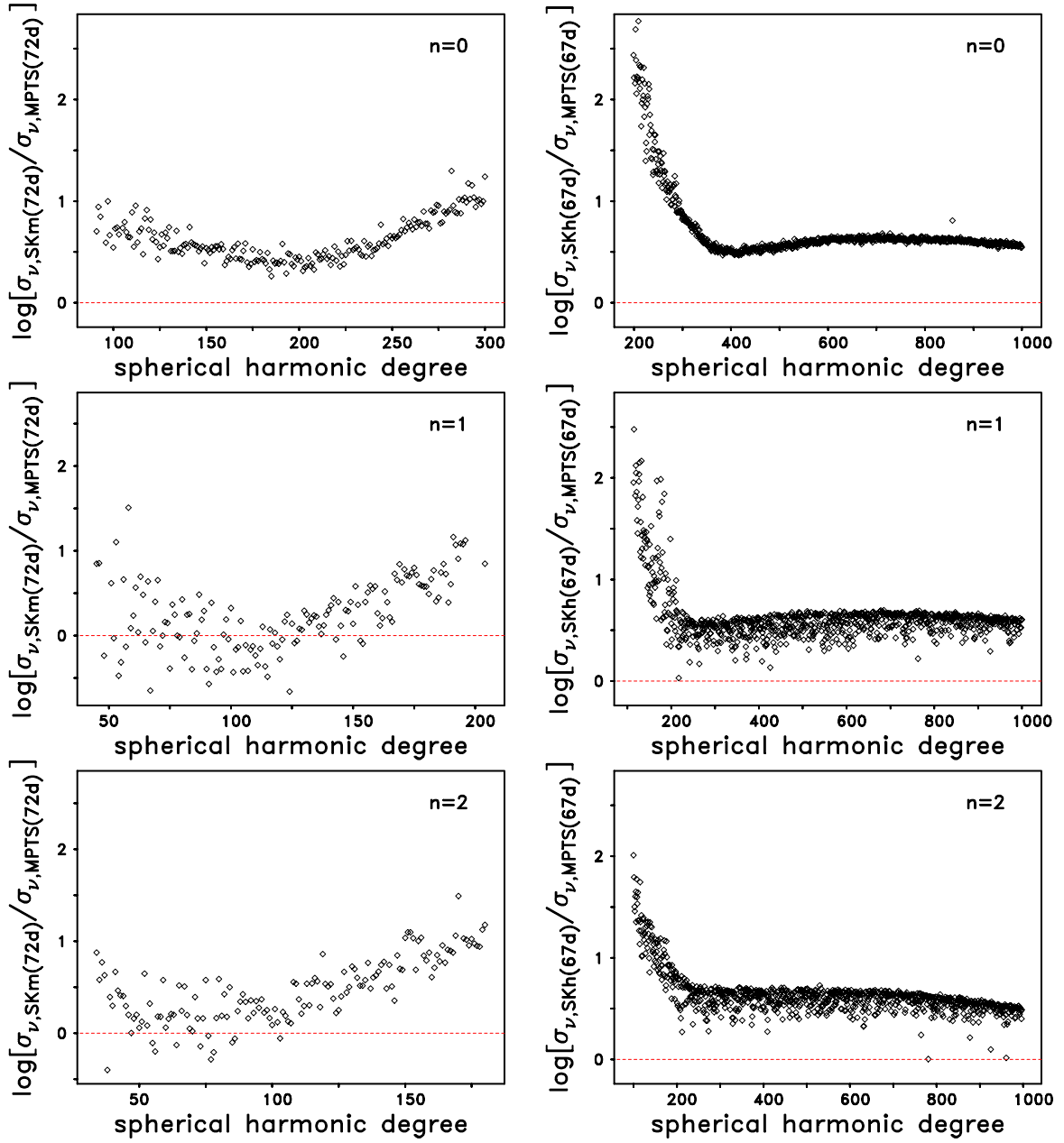
Figure 16. (Left-panels) Logarithm of the ratios of the SKm(72d) frequency uncertainties, $\sigma_{\nu,\mathrm{SKm(72d)}}$, to the corresponding MPTS(72d) frequency uncertainties, $\sigma_{\nu,\mathrm{MPTS(72d)}}$, as functions of the spherical harmonic degree for the $n = 0$ ridge (top), $n = 1$ ridge (middle), and $n = 2$ ridge (bottom). The horizontal dashed red line is for a ratio of unity. (Right panels) Same as left panels, but for the ratios of the SKh(67d) frequency uncertainties, $\sigma_{\nu,\mathrm{SKh(67d)}}$, to the corresponding MPTS(67d) frequency uncertainties, $\sigma_{\nu,\mathrm{MPTS(67d)}}$.

6. CONCLUSIONS

The success of helioseismology is essentially based on the possibility of performing numerical inversions of different properties of the solar oscillations. In terms of global helioseismology, one such type of inversion is the "structural inversion" in which tables of the frequencies of f- and p-mode oscillations and their associated uncertainties are employed to infer the structure of the solar interior. An important test of the reliability of the mode frequencies obtained from various fitting methodologies is that they are consistent with one another when applied to contemporaneous helioseismic observations. Here we have compared f- and p-mode frequencies obtained from the MPTS method (Reiter et al. 2020) with those obtained from the mean-multiplet technique (Schou 1992; Schou et al. 2002), the high-degree fitting methodology of Korzennik et al. (2004), the medium-degree fitting methodology of Korzennik (2005, 2008a,b), and the fitting methodology of the Birmingham Solar Oscillations Network group (Broomhall et al. 2009; Davies et al. 2014; Hale et al. 2016) using data based on 67-, 72-, and 90-day long time series of full-disk dopplergrams acquired by the HMI in 2010, and on low-degree Sun-as-a-star observations acquired by the ground-based observing stations of the BiSON group. While we have found excellent agreement between the MPTS, JS, SKm, and BR frequencies in the range of low and intermediate degrees, there are significant differences between the MPTS, JS and SKh frequencies in the range of intermediate and high degrees. We were able to demonstrate that the differences in the SKh(67d) and MPTS(67d) frequencies are not due to the use of invalid seed frequencies in the MPTS method. Rather, we could show that the MPTS method is able to accurately restore the MPTS(67d) frequencies when starting from the SKh(67d) frequencies for the lower-order ridges. Overall, we have shown that the MPTS fitting method provides frequencies that are in excellent agreement with other state-of-the-art fitting methods for degrees up to $l = 300$ and which are superior to the SKh method for degrees between $l = 301$ and 1350. The inclusion of large numbers of MPTS frequencies in this range of degrees should provide more precise estimates of solar internal structure in the range of depths incorporated in the Near-Surface Shear Layer.

REFERENCES

Anderson, E. R., Duvall, Thomas L., J., & Jefferies, S. M. 1990, ApJ, 364, 699, doi: 10.1086/169452

Basu, S. 2010, Ap&SS, 328, 43, doi: 10.1007/s10509-009-0201-9

—. 2016, Living Reviews in Solar Physics, 13, 2, doi: 10.1007/s41116-016-0003-4

Basu, S., Christensen-Dalsgaard, J., Howe, R., et al. 2003, ApJ, 591, 432, doi: 10.1086/375331

Broomhall, A. M., Chaplin, W. J., Davies, G. R., et al. 2009, MNRAS, 396, L100, doi: 10.1111/j.1745-3933.2009.00672.x

Chaplin, W. J., Elsworth, Y., Howe, R., et al. 1996, SoPh, 168, 1, doi: 10.1007/BF00145821

Christensen-Dalsgaard, J. 2002, Reviews of Modern Physics, 74, 1073, doi: 10.1103/RevModPhys.74.1073

Christensen-Dalsgaard, J., & Berthomieu, G. 1991, in Solar Interior and Atmosphere, 401–478

Davies, G. R., Broomhall, A. M., Chaplin, W. J., Elsworth, Y., & Hale, S. J. 2014, MNRAS, 439, 2025, doi: 10.1093/mnras/stu080

Di Mauro, M. P., Christensen-Dalsgaard, J., Rabello-Soares, M. C., & Basu, S. 2002, A&A, 384, 666, doi: 10.1051/0004-6361:20020020

Fossat, E. 1991, SoPh, 133, 1, doi: 10.1007/BF00149818

Gabriel, A. H., Charra, J., Grec, G., et al. 1997, SoPh, 175, 207, doi: 10.1023/A:1004911408285

Hale, S. J., Howe, R., Chaplin, W. J., Davies, G. R., & Elsworth, Y. P. 2016, SoPh, 291, 1, doi: 10.1007/s11207-015-0810-0

Harvey, J., Tucker, R., & Britanik, L. 1998, in ESA Special Publication, Vol. 418, Structure and Dynamics of the Interior of the Sun and Sun-like Stars, ed. S. Korzennik, 209–211

Harvey, J. W., Hill, F., Hubbard, R. P., et al. 1996, Science, 272, 1284, doi: 10.1126/science.272.5266.1284

Hill, F., Bolding, J., Toner, C., et al. 2003, in ESA Special Publication, Vol. 517, GONG+ 2002. Local and Global Helioseismology: the Present and Future, ed. H. Sawaya-Lacoste, 295–298

Howe, R., Chaplin, W. J., Elsworth, Y. P., et al. 2003, ApJ, 588, 1204, doi: 10.1086/374336

Howe, R., Davies, G. R., Chaplin, W. J., Elsworth, Y. P., & Hale, S. J. 2015, MNRAS, 454, 4120, doi: 10.1093/mnras/stv2210

Korzennik, S. G. 2005, ApJ, 626, 585, doi: 10.1086/429748

—. 2008a, Astronomische Nachrichten, 329, 453, doi: 10.1002/asna.200710979

Korzennik, S. G. 2008b, in Journal of Physics Conference Series, Vol. 118, Journal of Physics Conference Series, 012082, doi: 10.1088/1742-6596/118/1/012082

—. 2023, Frontiers in Astronomy and Space Sciences, 9, 1031313, doi: 10.3389/fspas.2022.1031313

Korzennik, S. G., Rabello-Soares, M. C., & Schou, J. 2004, ApJ, 602, 481, doi: 10.1086/381021

Korzennik, S. G., Rabello-Soares, M. C., Schou, J., & Larson, T. P. 2013, ApJ, 772, 87, doi: 10.1088/0004-637X/772/2/87

Kosovichev, A. G. 2009, in American Institute of Physics Conference Series, Vol. 1170, Stellar Pulsation: Challenges for Theory and Observation, ed. J. A. Guzik & P. A. Bradley, 547–559, doi: 10.1063/1.3246561

Larson, T. P., & Schou, J. 2015, SoPh, 290, 3221, doi: 10.1007/s11207-015-0792-y

—. 2018, SoPh, 293, 29, doi: 10.1007/s11207-017-1201-5

Nigam, R., & Kosovichev, A. G. 1998, ApJL, 505, L51, doi: 10.1086/311594

Reiter, J., Rhodes, E. J., J., Kosovichev, A. G., et al. 2020, ApJ, 894, 80, doi: 10.3847/1538-4357/ab7a17

—. 2015, ApJ, 803, 92, doi: 10.1088/0004-637X/803/2/92

Rhodes, E. J., J., Kosovichev, A. G., Schou, J., Scherrer, P. H., & Reiter, J. 1997, SoPh, 175, 287, doi: 10.1023/A:1004963425123

Scherrer, P. H., Bogart, R. S., Bush, R. I., et al. 1995, SoPh, 162, 129, doi: 10.1007/BF00733429

Schou, J. 1992, PhD thesis, Aarhus Univ.

Schou, J., Howe, R., Basu, S., et al. 2002, ApJ, 567, 1234, doi: 10.1086/338665

Schou, J., Scherrer, P. H., Bush, R. I., et al. 2012, SoPh, 275, 229, doi: 10.1007/s11207-011-9842-2

Woodard, M. F. 1989, ApJ, 347, 1176, doi: 10.1086/168206